Electronic Journal of Differential Equations, Vol. 2026 (2026), No. 69, pp. 1–24.
ISSN: 1072-6691. URL: https://ejde.math.txstate.edu, DOI: 10.58997/ejde.2026.69

DYNAMICAL ANALYSIS OF A THREE-COMMUNITY MODEL FOR MALWARE TRANSMISSION

ZIHENG CHENG, HANQING HU, TENG MA, HUANGJIE ZHENG

Abstract. Malware transmission remains a serious threat to computer networks, particularly in heterogeneous environments. We propose a three community SIP model (Susceptible-Infected-Protected) that includes both intra and intercommunity transmissions. The basic reproduction number $\mathcal{R}_0$ is derived using the next-generation matrix method and serves as the threshold between extinction and persistence of malware. Analysis shows that the malware-free equilibrium is globally stable when $\mathcal{R}_0 < 1$, while an endemic equilibrium exists and remains stable when $\mathcal{R}_0 > 1$. Numerical results support the theory and highlight that stronger protection and limited cross-community connections can effectively suppress malware spread.

1. Introduction

The Internet has become an integral part of modern human life. We rely on it almost everywhere we go—to stay connected with family and friends, access information, and keep up to date with global news. However, alongside the rapid advancement of Internet technologies over the past few decades, the threats posed by malware and online rumors have grown increasingly severe. As a result, the security of legitimate networks is constantly under threat.

Malware, short for malicious software, refers to programs intentionally designed to disrupt, damage, or gain unauthorized access to computer systems. Common types include worms that replicate autonomously, ransomware that encrypts user data for extortion, and botnets that hijack large numbers of devices for coordinated attacks [2, 8]. Over the past two decades, outbreaks such as Code Red (2001) [32], WannaCry (2017) [1], and NotPetya (2017) [15] have demonstrated how rapidly malicious code can spread across global networks, causing enormous economic and security losses [28]. Given the increasing interdependence of digital infrastructures, understanding the transmission dynamics of malware has become essential for designing effective defense mechanisms.

From a security perspective, the malware spreading phenomenon is analogous to an epidemic process [3], in which informed nodes disseminate malicious information to their neighbors [23]. To study these dynamics, researchers have adapted epidemiological models from mathematical biology [13]. Traditional epidemic models such as SI, SIS [22], SIR [20] and SIRS [16] classify individuals into compartments (susceptible, infected, recovered) and describe transitions between these states. By analogy, the computer nodes in a network can be modeled and analyzed in a similar way [5, 7, 25].

However, the transmission dynamics of computer malware differ fundamentally from human biological diseases. In human epidemics, recovered individuals typically develop antibodies, granting them temporary or permanent natural immunity against reinfection. In contrast, when a compromised computer is disinfected and the malware is removed, it does not acquire any natural immunity; instead, it immediately reverts to the susceptible state, facing an instant risk of reinfection [19]. To effectively mitigate this risk, computer networks must rely on artificial defense mechanisms such as firewalls, security patches, and intrusion prevention systems [9, 14, 26]. Consequently, in this study, we adopt the SIP model, consisting of the susceptible (S), infected

2020 *Mathematics Subject Classification.* 34D20, 65L07, 92D30.
Key words and phrases. Malware transmission; susceptible-infected-protected model; reproduction number.

Submitted Mach 25, 2026. Published September 10, 2026.

(I) and protected (P) nodes. Susceptible nodes (S) are vulnerable to infection, infected nodes (I) actively spread malware, protected (P) state explicitly characterizes nodes that are selected and fortified by these network defense mechanisms. Unlike the 'recovered' state in traditional epidemiological models, the protected state emphasizes technical defense and immunization, capturing the fact that protection may degrade over time and therefore differs from permanent recovery. This framework provides a more realistic representation of the defense of a computer network.

While previous studies have explored malware propagation using various compartmental models, they predominantly focus on homogeneous settings or single, isolated networks [4, 11, 29]. Real-world digital infrastructures, however, are fundamentally compartmentalized into interconnected subnetworks or communities [17, 21] such as corporate departments, university faculties, geographically distributed data centers, or even national networks subject to cross-border restrictions. These communities typically exhibit heterogeneous connectivity patterns and protection policies. Malware transmission in such environments is strongly influenced by intercommunity links, which may act either as channels that accelerate spread or as barriers that mitigate transmission [6]. To the best of our knowledge, this study is the first to establish a realistic three-community SIP model that comprehensively captures both intra-community and inter-community malware transmission dynamics. Furthermore, this mathematical framework is highly scalable and can be generalized to scenarios involving an arbitrary number of communities. By seamlessly integrating structural heterogeneity and realistic defense mechanisms, our work provides a valid, rigorous, and adaptable theoretical environment for analyzing malware propagation and designing targeted security interventions in complex network topologies.

A central concept in epidemic modeling is the basic reproduction number $\mathcal{R}_0$, which quantifies the expected number of new infections caused by a single infected node in a fully susceptible environment [10]. For malware transmission, $\mathcal{R}_0$ serves as a threshold: if $\mathcal{R}_0 < 1$, malware dies out; if $\mathcal{R}_0 > 1$, infection can persist and potentially spread across all communities[27]. By analyzing the next-generation matrix associated with the three-community system SIP, we derive $\mathcal{R}_0$ and use it to evaluate the conditions under which malware outbreaks can be prevented or controlled. To complement the theoretical results, numerical simulations are conducted, illustrating how heterogeneity influences transmission speed, outbreak size, and long-term persistence. Simulations also highlight how strengthening community-specific protection measures or reducing cross-community infection rates can effectively reduce $\mathcal{R}_0$ and drive the system toward eradication of malware.

The remainder of this paper is organized as follows: Section 2 describes the three-community SIP model, including assumptions, parameter definitions, the heterogeneous mean-field degree formulation, and the full system of equations. Section 3 presents the main analytical results: positivity and invariance of solutions, derivation of the next-generation matrix and the basic reproduction number $\mathcal{R}_0$ (with the characteristic-polynomial reduction into $P(\lambda)$ and $Q(\lambda)$), and stability analysis of the disease-free equilibrium. Section 4 provides numerical simulations.

2. Model description

When studying malware transmission on networks, computers or devices are represented as nodes, and the communication links among them are represented as edges. In the context of multiple communities, each community can be viewed as a subnetwork, while inter-community connections capture cross-community interactions such as the use of USB devices, VPN access, or other data exchanges.

To precisely characterize the structural connectivity within each subnetwork, we adopt the foundational concept of "degree" from network science. The degree k of a node is defined as the number of adjacent nodes directly connected to it (i.e., its immediate neighbors). In real-world network scenarios, this concept maps naturally to various systems: for instance, in the World Wide Web, the degree of a website represents the number of other sites linked to it via hyperlinks; in a computer network, it corresponds to the number of devices—such as other computers, servers, or data transmission peripherals like USB drives—directly connected to a specific host machine. Given that real-world networks exhibit varying scales and levels of structural complexity, node degrees can span a wide range and become exceptionally large in complex topologies. To accommodate

this structural heterogeneity while maintaining mathematical tractability, we introduce n_A, n_B, and n_C to represent the maximum node degree within subnetworks A, B, and C, respectively. Consequently, the range of the degree k for any node in community $X \in \{A, B, C\}$ is bounded by $1 \leq k \leq n_X$, where the exact value of the upper bound n_X is intrinsically determined by the specific empirical network under consideration.

Malware transmission can be categorized into intra-community and inter- community processes. For intra-community transmission, we adopt the heterogeneous mean-field theory, which assumes that nodes with the same degree are statistically equivalent and equally likely to connect with one another. For inter-community transmission, we assume that all nodes within a community have the same risk of infection and the same probability of exposure when interacting with infected nodes from other communities.

We now consider a three-community system, where each node can exist in one of three possible states: Susceptible (S), Infected (I), or Protected (P). Susceptible nodes are vulnerable to infection, infected nodes are both compromised by malware and capable of spreading it, and protected nodes are temporarily immune until their protection expires. We assume that the defense mechanism of each subnetwork selects nodes to be protected with a fixed probability at each time step, regardless of their degree. Protected nodes lose their protection at a uniform rate and return to the susceptible state. The inter-community transmission and intra-community transmission processes are illustrated in the following figure.

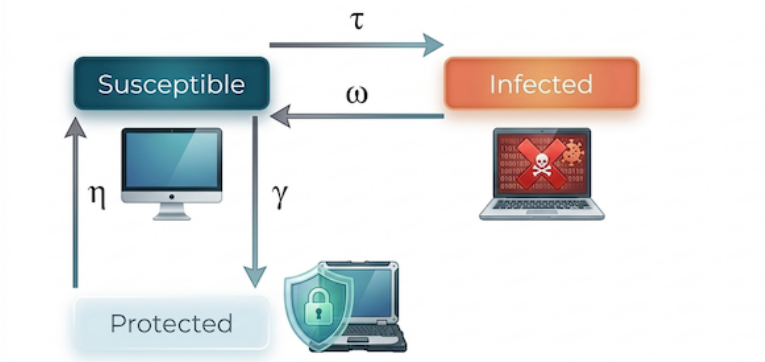

FIGURE 1. Intra-community Transition

According to our previous heterogeneous mean-field assumption, we can view the nodes in the same community with the same degree and in the same state as equivalent. Thus, we let s_k^A denote the density of susceptible nodes with degree k in community A, i_k^A the density of infected nodes with degree k in community A, and p_k^A the density of protected nodes with degree k in community A. Similarly, we define s_k^B, i_k^B, p_k^B for community B, and s_k^C, i_k^C, p_k^C for community C.Since we aim to consider both inter-community and intra-community transmissions, we introduce α_1 as the proportion of inter-community transmission between B and A, α_2 as that between C and A, β_1 as that between C and B, β_2 as that between A and B, δ_1 as that between A and C, and δ_2 as that between B and C. Therefore, the proportions of intra-community transmission are given by $1 - \alpha_1 - \alpha_2$ for community A, $1 - \beta_1 - \beta_2$ for community B, and $1 - \delta_1 - \delta_2$ for community C.

Now we have constructed the model based on our assumptions. The parameters of this model are listed in Table 1.

Table 1: *Description of the model parameters.*

Parameter	**Description**
$\tau_A > 0$	Transmission probability from an infected node to a susceptible node in community A through network contact.

Parameter	Description
$\tau_B > 0$	Transmission probability from an infected node to a susceptible node in community B through network contact.
$\tau_C > 0$	Transmission probability from an infected node to a susceptible node in community C through network contact.
$\sigma_{BA} > 0$	Transmission probability from an infected node in community B to a susceptible node in community A through inter-community contact.
$\sigma_{AB} > 0$	Transmission probability from an infected node in community A to a susceptible node in community B through inter-community contact.
$\sigma_{CB} > 0$	Transmission probability from an infected node in community C to a susceptible node in community B through inter-community contact.
$\sigma_{BC} > 0$	Transmission probability from an infected node in community B to a susceptible node in community C through inter-community contact.
$\sigma_{AC} > 0$	Transmission probability from an infected node in community A to a susceptible node in community C through inter-community contact.
$\sigma_{CA} > 0$	Transmission probability from an infected node in community C to a susceptible node in community A through inter-community contact.
$\omega_A > 0$	Recovery rate of infected nodes in community A.
$\omega_B > 0$	Recovery rate of infected nodes in community B.
$\omega_C > 0$	Recovery rate of infected nodes in community C.
$\gamma_A > 0$	Immunization rate of susceptible nodes in community A.
$\gamma_B > 0$	Immunization rate of susceptible nodes in community B.
$\gamma_C > 0$	Immunization rate of susceptible nodes in community C.
$\eta_A > 0$	Rate at which protected nodes lose protection in community A.
$\eta_B > 0$	Rate at which protected nodes lose protection in community B.
$\eta_C > 0$	Rate at which protected nodes lose protection in community C.
$0 \le \alpha_1 \le 1$	Contribution of malware transmission from community B to community A.
$0 \le \alpha_2 \le 1$	Contribution of malware transmission from community C to community A.
$1 - \alpha_1 - \alpha_2$	Contribution of malware transmission within community A.
$0 \le \beta_1 \le 1$	Contribution of malware transmission from community C to community B.
$0 \le \beta_2 \le 1$	Contribution of malware transmission from community A to community B.
$1 - \beta_1 - \beta_2$	Contribution of malware transmission within community B.
$0 \le \delta_1 \le 1$	Contribution of malware transmission from community A to community C.
$0 \le \delta_2 \le 1$	Contribution of malware transmission from community B to community C.
$1 - \delta_1 - \delta_2$	Contribution of malware transmission within community C.

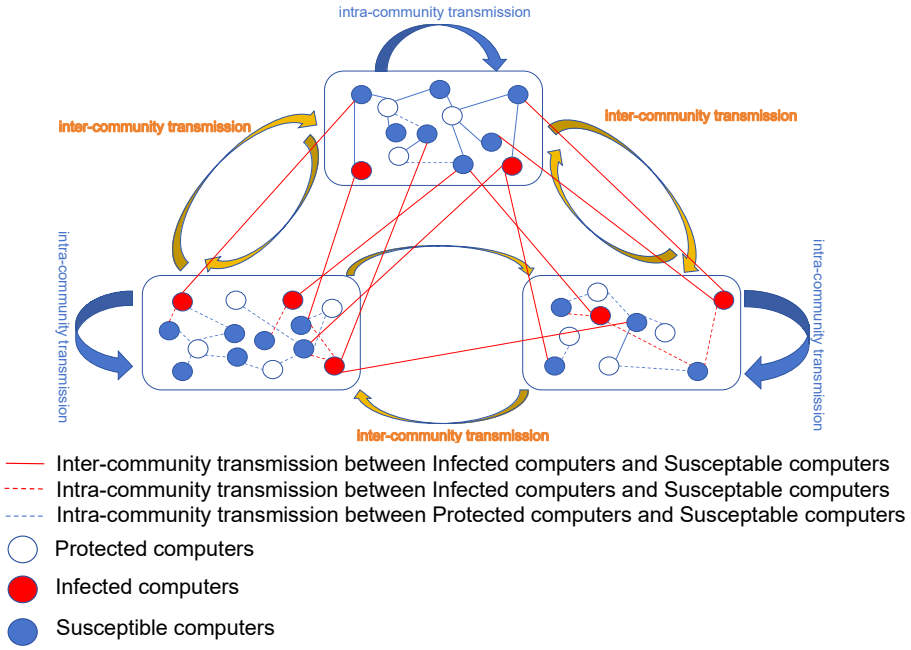

FIGURE 2. Transmissions

The equations of the system based on our model are as follows:

$$\begin{aligned}
\dot{s}_k^A &= -\alpha_1\sigma_{BA}s_k^A i_B - \alpha_2\sigma_{CA}s_k^A i_C - (1-\alpha_1-\alpha_2)k\tau_A s_k^A\Theta_i^A - \gamma_A s_k^A + \eta_A p_k^A + \omega_A i_k^A\\
\dot{i}_k^A &= \alpha_1\sigma_{BA}s_k^A i_B + \alpha_2\sigma_{CA}s_k^A i_C + (1-\alpha_1-\alpha_2)k\tau_A s_k^A\Theta_i^A - \omega_A i_k^A\\
\dot{p}_k^A &= \gamma_A s_k^A - \eta_A p_k^A\\
\dot{s}_k^B &= -\beta_1\sigma_{CB}s_k^B i_C - \beta_2\sigma_{AB}s_k^B i_A - (1-\beta_1-\beta_2)k\tau_B s_k^B\Theta_i^B - \gamma_B s_k^B + \eta_B p_k^B + \omega_B i_k^B\\
\dot{i}_k^B &= \beta_1\sigma_{CB}s_k^B i_C + \beta_2\sigma_{AB}s_k^B i_A + (1-\beta_1-\beta_2)k\tau_B s_k^B\Theta_i^B - \omega_B i_k^B\\
\dot{p}_k^B &= \gamma_B s_k^B - \eta_B p_k^B\\
\dot{s}_k^C &= -\delta_1\sigma_{AC}s_k^C i_A - \delta_2\sigma_{BC}s_k^C i_B - (1-\delta_1-\delta_2)k\tau_C s_k^C\Theta_i^C\\
&\quad - \gamma_C s_k^C + \eta_C p_k^C + \omega_C i_k^C\\
\dot{i}_k^C &= \delta_1\sigma_{AC}s_k^C i_A + \delta_2\sigma_{BC}s_k^C i_B + (1-\delta_1-\delta_2)k\tau_C s_k^C\Theta_i^C - \omega_C i_k^C\\
\dot{p}_k^C &= \gamma_C s_k^C - \eta_C p_k^C
\end{aligned} \tag{2.1}$$

where $\langle j\rangle_A = \sum_j jP_j^A$ denotes the expectation of how many edges one node has in the sub-network of community A and $\Theta_i^A = \frac{\sum_j jP_j^A i_j^A}{\langle j\rangle_A}$ denotes the probability that a randomly chosen edge in the sub-network of community A points to an infected node within the same community . Similarly,

$$\Theta_i^B = \frac{\sum_k kP_k^B i_k^B}{\langle k\rangle_B}, \langle k\rangle_B = \sum_k kP_k^B, \Theta_i^C = \frac{\sum_l lP_l^C i_l^C}{\langle l\rangle_C}, \langle l\rangle_C = \sum_l lP_l^C \tag{2.2}$$

represent the corresponding expectations and probabilities for communities B and C, respectively.

The total density of infected nodes in each community is defined as

$$i_A = \sum_j P_j^A i_j^A, i_B = \sum_k P_k^B i_k^B, i_C = \sum_l P_l^C i_l^C, \tag{2.3}$$

where P_j^A, P_k^B, and P_l^C denote the degree distributions of communities A, B, and C, respectively.

Since $i_A = \sum_j P_j^A i_j^A$, we have $\dot{i}_A = \sum_j P_j^A \dot{i}_j^A$. Given that $\dot{i}_j^A = \alpha_1\sigma_{BA}s_j^A i_B + \alpha_2\sigma_{CA}s_j^A i_C + (1-\alpha_1-\alpha_2)j\tau_A s_j^A\Theta_i^A - \omega_A i_j^A$ we obtain

$$\dot{i}_A = \alpha_1\sigma_{BA}s_A i_B + \alpha_2\sigma_{CA}s_A i_C + (1-\alpha_1-\alpha_2)\langle j\rangle_A\tau_A\Theta_s^A\Theta_i^A - \omega_A i_A,$$

where $\Theta_s^A = \frac{\sum_j jP_j^A s_j^A}{\langle j\rangle_A}, s_A = \sum_j P_j^A s_j^A$.

Similarly, since $\Theta_i^A = \frac{\sum_j jP_j^A i_j^A}{\langle j\rangle_A}$ we can derive

$$\dot{\Theta}_i^A = \alpha_1\sigma_{BA}\Theta_s^A i_B + \alpha_2\sigma_{CA}\Theta_s^A i_C + (1-\alpha_1-\alpha_2)\tau_A\frac{\sum_j j^2P_j^A s_j^A}{\langle j\rangle_A}\Theta_i^A - \omega_A\Theta_i^A.$$

In the same way, for communities B and C, we have

$$\begin{aligned}
\dot{i}_B &= \beta_1\sigma_{CB}s_B i_C + \beta_2\sigma_{AB}s_B i_A + (1-\beta_1-\beta_2)\langle k\rangle_B\tau_B\Theta_s^B\Theta_i^B - \omega_B i_B,\\
\dot{\Theta}_i^B &= \beta_1\sigma_{CB}\Theta_s^B i_C + \beta_2\sigma_{AB}\Theta_s^B i_A + (1-\beta_1-\beta_2)\tau_B\frac{\sum_k k^2P_k^B s_k^B}{\langle k\rangle_B}\Theta_i^B - \omega_B\Theta_i^B,\\
\dot{i}_C &= \delta_1\sigma_{AC}s_C i_A + \delta_2\sigma_{BC}s_C i_B + (1-\delta_1-\delta_2)\langle l\rangle_C\tau_C\Theta_s^C\Theta_i^C - \omega_C i_C,\\
\dot{\Theta}_i^C &= \delta_1\sigma_{AC}\Theta_s^C i_A + \delta_2\sigma_{BC}\Theta_s^C i_B + (1-\delta_1-\delta_2)\tau_C\frac{\sum_l l^2P_l^C s_l^C}{\langle l\rangle_C}\Theta_i^C - \omega_C\Theta_i^C.
\end{aligned}$$

where

$$\Theta_s^B = \frac{\sum_k kP_k^B s_k^B}{\langle k\rangle_B}, s_B = \sum_k P_k^B s_k^B, \Theta_s^C = \frac{\sum_l lP_l^C s_l^C}{\langle l\rangle_C}, s_C = \sum_l P_l^C s_l^C.$$

We list the meanings of these newly emerged variables in Table **??**.

Table 2: Description of some newly variables.

Variable	**Description**
P_j^A	Distribution of nodes with degree j in the sub-network of community A.
P_k^B	Distribution of nodes with degree k in the sub-network of community B.
P_l^C	Distribution of nodes with degree l in the sub-network of community C.
i_A	Total density of infected nodes in community A.
i_B	Total density of infected nodes in community B.
i_C	Total density of infected nodes in community C.
s_A	Total density of susceptible nodes in community A.
s_B	Total density of susceptible nodes in community B.
s_C	Total density of susceptible nodes in community C.
$\langle j\rangle_A$	Expectation of how many edges one node has in the sub-network of community A.
$\langle k\rangle_B$	Expectation of how many edges one node has in the sub-network of community B.
$\langle l\rangle_C$	Expectation of how many edges one node has in the sub-network of community C.
Θ_i^A	Probability that a randomly chosen edge in the sub-network of community A points to an infected node within the same community.
Θ_i^B	Probability that a randomly chosen edge in the sub-network of community B points to an infected node within the same community.
Θ_i^C	Probability that a randomly chosen edge in the sub-network of community C points to an infected node within the same community.
Θ_s^A	Probability that a randomly chosen edge in the sub-network of community A points to an infected node within the same community.

Variable	Description
Θ_s^B	Probability that a randomly chosen edge in the sub-network of community B points to an infected node within the same community.
Θ_s^C	Probability that a randomly chosen edge in the sub-network of community C points to an infected node within the same community.

Putting together the equations mentioned above, we have:

$$\begin{aligned}
\dot{i}_A &= \alpha_1\sigma_{BA}s_A i_B + \alpha_2\sigma_{CA}s_A i_C + (1-\alpha_1-\alpha_2)\langle j\rangle_A\tau_A\Theta_s^A\Theta_i^A - \omega_A i_A,\\
\dot{i}_B &= \beta_1\sigma_{CB}s_B i_C + \beta_2\sigma_{AB}s_B i_A + (1-\beta_1-\beta_2)\langle k\rangle_B\tau_B\Theta_s^B\Theta_i^B - \omega_B i_B,\\
\dot{i}_C &= \delta_1\sigma_{AC}s_C i_A + \delta_2\sigma_{BC}s_C i_B + (1-\delta_1-\delta_2)\langle l\rangle_C\tau_C\Theta_s^C\Theta_i^C - \omega_C i_C,\\
\dot{\Theta}_i^A &= \alpha_1\sigma_{BA}\Theta_s^A i_B + \alpha_2\sigma_{CA}\Theta_s^A i_C + (1-\alpha_1-\alpha_2)\tau_A\frac{\sum_j j^2P_j^A s_j^A}{\langle j\rangle_A}\Theta_i^A - \omega_A\Theta_i^A,\\
\dot{\Theta}_i^B &= \beta_1\sigma_{CB}\Theta_s^B i_C + \beta_2\sigma_{AB}\Theta_s^B i_A + (1-\beta_1-\beta_2)\tau_B\frac{\sum_k k^2P_k^B s_k^B}{\langle k\rangle_B}\Theta_i^B - \omega_B\Theta_i^B,\\
\dot{\Theta}_i^C &= \delta_1\sigma_{AC}\Theta_s^C i_A + \delta_2\sigma_{BC}\Theta_s^C i_B + (1-\delta_1-\delta_2)\tau_C\frac{\sum_l l^2P_l^C s_l^C}{\langle l\rangle_C}\Theta_i^C - \omega_C\Theta_i^C.
\end{aligned} \tag{2.4}$$

3. Main results

This section focuses on the dynamical analysis of the proposed model, including the proof of solution positivity and the derivation of the basic reproduction number.

3.1. **Positivity of solutions.** The following analysis concerns the *positivity* of the proposed model. For simplicity, the differential equations governing the susceptible computers are omitted(because the total number of devices in the community remains unchanged), and we focus instead on the relative densities of the protected and infected nodes. Define the state vector

$$\begin{aligned}
\vec{Y}(t) = \Big(& \underbrace{i_1^A, i_2^A, \dots, i_{n_A}^A}_{\text{infected in community A}} \quad , \quad \underbrace{p_1^A, \dots, p_{n_A}^A}_{\text{protected in community A}} \quad ,\\
& \underbrace{i_1^B, \dots, i_{n_B}^B}_{\text{infected in community B}} \quad , \quad \underbrace{p_1^B, \dots, p_{n_B}^B}_{\text{protected in community B}} \quad ,\\
& \underbrace{i_1^C, \dots, i_{n_C}^C}_{\text{infected in community C}} \quad , \quad \underbrace{p_1^C, \dots, p_{n_C}^C}_{\text{protected in community C}} \quad \Big)^T,
\end{aligned}$$

which collects the densities of infected and protected computers in all communities at time t. Obviously, the components of the state vector $\vec{Y}(t)$ correspond to the variables of the three communities as follows:

$$\begin{aligned}
Y_k &= i_k^A(t), \quad k = 1, \dots, n_A,\\
Y_{k+n_A} &= p_k^A(t), \quad k = 1, \dots, n_A,\\
Y_{l+2n_A} &= i_l^B(t), \quad l = 1, \dots, n_B,\\
Y_{l+2n_A+n_B} &= p_l^B(t), \quad l = 1, \dots, n_B,\\
Y_{m+2n_A+2n_B} &= i_m^C(t), \quad m = 1, \dots, n_C,\\
Y_{m+2n_A+2n_B+n_C} &= p_m^C(t), \quad m = 1, \dots, n_C.
\end{aligned}$$

Theorem 3.1. *If the initial value of system* (2.1) *satisfies*

$$\vec{Y}(0) \in \Lambda_{2(n_A+n_B+n_C)} = \prod_{i=1}^{2(n_A+n_B+n_C)} [0,1],$$

then for any $t > 0$, we have

$$\vec{Y}(t) \in \Lambda_{2(n_A+n_B+n_C)}.$$

Moreover, $\Lambda_{3(n_A+n_B+n_C)}$ is a positively invariant set of system (2.1).

Proof. First, define the boundary of the region $\Lambda_{2(n_A+n_B+n_C)}$ as

$$\partial\Lambda^1 = \big\{\vec{Y}(t) \in \Lambda_{2(n_A+n_B+n_C)} : Y_i = 0 \text{ for some } i\big\},$$
$$\partial\Lambda^2 = \big\{\vec{Y}(t) \in \Lambda_{2(n_A+n_B+n_C)} : Y_i = 1 \text{ for some } i\big\}.$$

According to [30], if a compact set Ω is invariant for the system $\dot{x} = f(x)$, then for all $x \in \partial\Omega$, the vector field $f(x)$ does not point strictly outward, i.e., its projection along the outward normal vector is nonpositive (it points inward or is zero).

In one-dimensional cases, the outward normal vectors are defined as

$$\xi^{\mathbf{1}}_{\mathbf{i}} = -\xi^{\mathbf{2}}_{\mathbf{i}} = (\overbrace{0, \dots, -1}^{i}, \dots, 0),$$

where $\xi^{\mathbf{1}}_{\mathbf{i}}$ corresponds to the boundary $Y_i = 0$, and $\xi^{\mathbf{2}}_{\mathbf{i}}$ corresponds to $Y_i = 1$.

Using system (2.1), we compute the inner product on the boundary $\partial\Lambda^1$ as follows:

$$\begin{aligned}
\frac{d\vec{Y}}{dt}\Big|_{Y_i=0} \cdot \xi^1_i &= -(1 - Y_{i+n_A})\Big[\alpha_1\sigma_{BA}\sum_{\substack{j=1\\ j\neq i}}^{n_B} P^B_j Y_{j+2n_A} + \alpha_2\sigma_{CA}\sum_{\substack{j=1\\ j\neq i}}^{n_C} P^C_j Y_{j+2n_A+2n_B} \\
&\quad + \frac{(1-\alpha_1-\alpha_2)i\tau_A}{\langle k\rangle_A}\sum_{\substack{j=1\\ j\neq i}}^{n_A} jP^A_j Y_j\Big] \le 0, \quad i = 1, \dots, n_A,
\end{aligned}$$

$$\frac{d\vec{Y}}{dt}\Big|_{Y_i=0} \cdot \xi^1_i = -\gamma_A(1 - Y_{i-n_A}) \le 0, \quad i = n_A+1, \dots, 2n_A,$$

$$\begin{aligned}
\frac{d\vec{Y}}{dt}\Big|_{Y_i=0} \cdot \xi^1_i &= -(1 - Y_{i+n_B})\Big[\beta_1\sigma_{CB}\sum_{\substack{j=1\\ j\neq i}}^{n_C} P^C_j Y_{j+2n_A+2n_B} + \beta_2\sigma_{AB}\sum_{\substack{j=1\\ j\neq i}}^{n_A} P^A_j Y_j \\
&\quad + \frac{(1-\beta_1-\beta_2)i\tau_B}{\langle k\rangle_B}\sum_{\substack{j=1\\ j\neq i}}^{n_B} jP^B_j Y_{j+2n_A}\Big] \le 0, \quad i = 2n_A+1, \dots, 2n_A+n_B,
\end{aligned}$$

$$\frac{d\vec{Y}}{dt}\Big|_{Y_i=0} \cdot \xi^1_i = -\gamma_B(1 - Y_{i-n_B}) \le 0, \quad i = 2n_A+n_B+1, \dots, 2n_A+2n_B,$$

$$\begin{aligned}
\frac{d\vec{Y}}{dt}\Big|_{Y_i=0} \cdot \xi^1_i &= -(1 - Y_{i+n_C})\Big[\delta_1\sigma_{AC}\sum_{\substack{j=1\\ j\neq i}}^{n_A} P^A_j Y_j + \delta_2\sigma_{BC}\sum_{\substack{j=1\\ j\neq i}}^{n_B} P^B_j Y_{j+2n_A} \\
&\quad + \frac{(1-\delta_1-\delta_2)i\tau_C}{\langle k\rangle_C}\sum_{\substack{j=1\\ j\neq i}}^{n_C} jP^C_j Y_{j+2n_A+2n_B}\Big] \le 0, \\
&\quad i = 2n_A+2n_B+1, \dots, 2n_A+2n_B+n_C,
\end{aligned}$$

$$\frac{d\vec{Y}}{dt}\Big|_{Y_i=0} \cdot \xi^1_i = -\gamma_C(1 - Y_{i-n_C}) \le 0, \quad i = 2n_A+2n_B+n_C+1, \dots, 2(n_A+n_B+n_C).$$

Similarly, on $\partial\Lambda^2$ we have:

$$\frac{d\vec{Y}}{dt}\Big|_{Y_i=1} \cdot \xi^2_i = -\omega_A < 0, \quad i = 1, \dots, n_A,$$
$$\frac{d\vec{Y}}{dt}\Big|_{Y_i=1} \cdot \xi^2_i = 0, \quad i = n_A+1, \dots, 2n_A,$$

$$\frac{d\vec{Y}}{dt}\Big|_{Y_i=1}\cdot\xi_i^2=-\omega_B<0,\quad i=2n_A+1,\dots,2n_A+n_B,$$
$$\frac{d\vec{Y}}{dt}\Big|_{Y_i=1}\cdot\xi_i^2=0,\quad i=2n_A+n_B+1,\dots,2n_A+2n_B,$$

$$\frac{d\vec{Y}}{dt}\Big|_{Y_i=1}\cdot\xi_i^2=-\omega_C<0,\quad i=2n_A+2n_B+1,\dots,2n_A+2n_B+n_C,$$
$$\frac{d\vec{Y}}{dt}\Big|_{Y_i=1}\cdot\xi_i^2=0,\quad i=2n_A+2n_B+n_C+1,\dots,2(n_A+n_B+n_C).$$

Therefore, for any initial condition

$$\vec{Y}(0)\in\Lambda_{2(n_A+n_B+n_C)}=\prod_{i=1}^{2(n_A+n_B+n_C)}[0,1],$$

the trajectory satisfies

$$\vec{Y}(t)\in\Lambda_{2(n_A+n_B+n_C)}=\prod_{i=1}^{2(n_A+n_B+n_C)}[0,1],$$

for all $t>0$. Moreover, since $i_k^X+s_k^X+p_k^X=1$ for $X\in\{A,B,C\}$, we have $s_k^X\in[0,1]$. Thus, the solution of system (2.1) remains within the region $\Lambda_{3(n_A+n_B+n_C)}$ for all $t>0$. This demonstrates that $\Lambda_{3(n_A+n_B+n_C)}$ is a positively invariant set of system (2.1). □

3.2. **Basic reproduction number and stability of the disease-free equilibrium.** Linearizing the system around the disease-free equilibrium (DFE), we obtain the compact matrix representation

$$\dot{\mathbf{w}}=(\mathbf{F}-\mathbf{V})\,\mathbf{w},\quad \mathbf{w}=\begin{pmatrix}i_A & i_B & i_C & \Theta_i^A & \Theta_i^B & \Theta_i^C\end{pmatrix}^T,\tag{3.1}$$

where $\mathbf{F}$ and $\mathbf{V}$ are the transmission and transition matrices, respectively. At the DFE, because of $\dot{p}_k^A=\dot{p}_k^B=\dot{p}_k^C=0$, the susceptible densities satisfy

$$s_j^A=\frac{\eta_A}{\eta_A+\gamma_A},\quad s_k^B=\frac{\eta_B}{\eta_B+\gamma_B},\quad s_l^C=\frac{\eta_C}{\eta_C+\gamma_C}.$$

Accordingly, the transmission matrix is

$$\mathbf{F}=\begin{pmatrix}
0 & \alpha_1 f_A\sigma_{BA} & \alpha_2 f_A\sigma_{CA} & \tilde{\alpha} f_A\tau_A\langle j\rangle_A & 0 & 0\\
\beta_2 f_B\sigma_{AB} & 0 & \beta_1 f_B\sigma_{CB} & 0 & \tilde{\beta} f_B\tau_B\langle k\rangle_B & 0\\
\delta_1 f_C\sigma_{AC} & \delta_2 f_C\sigma_{BC} & 0 & 0 & 0 & \tilde{\delta} f_C\tau_C\langle l\rangle_C\\
0 & \alpha_1 f_A\sigma_{BA} & \alpha_2 f_A\sigma_{CA} & \tilde{\alpha} f_A\tau_A\frac{\langle j^2\rangle_A}{\langle j\rangle_A} & 0 & 0\\
\beta_2 f_B\sigma_{AB} & 0 & \beta_1 f_B\sigma_{CB} & 0 & \tilde{\beta} f_B\tau_B\frac{\langle k^2\rangle_B}{\langle k\rangle_B} & 0\\
\delta_1 f_C\sigma_{AC} & \delta_2 f_C\sigma_{BC} & 0 & 0 & 0 & \tilde{\delta} f_C\tau_C\frac{\langle l^2\rangle_C}{\langle l\rangle_C}
\end{pmatrix}\tag{3.2}$$

with

$$f_X=\frac{\eta_X}{\eta_X+\gamma_X}\quad X\in\{A,B,C\}\quad \tilde{\alpha}=1-\alpha_1-\alpha_2,\quad \tilde{\beta}=1-\beta_1-\beta_2,\quad \tilde{\delta}=1-\delta_1-\delta_2,$$
$$\mathbf{V}=\operatorname{diag}(\omega_A,\omega_B,\omega_C,\omega_A,\omega_B,\omega_C).$$

Following the next-generation matrix approach, the basic reproduction number is

$$\mathcal{R}_0=\rho(\mathbf{F}\mathbf{V}^{-1}),$$

where $\rho(\cdot)$ denotes the spectral radius. Introducing the block decomposition

$$\mathbf{F}=\begin{pmatrix}\mathbf{M} & \mathbf{D}_1\\ \mathbf{M} & \mathbf{D}_2\end{pmatrix},\quad \mathbf{K}=\mathbf{F}\mathbf{V}^{-1}=\begin{pmatrix}\mathbf{M}\mathbf{V}_1^{-1} & \mathbf{D}_1\mathbf{V}_2^{-1}\\ \mathbf{M}\mathbf{V}_1^{-1} & \mathbf{D}_2\mathbf{V}_2^{-1}\end{pmatrix},$$

with

$$\mathbf{M} = \begin{pmatrix} 0 & \alpha_1 f_A \sigma_{BA} & \alpha_2 f_A \sigma_{CA} \\ \beta_2 f_B \sigma_{AB} & 0 & \beta_1 f_B \sigma_{CB} \\ \delta_1 f_C \sigma_{AC} & \delta_2 f_C \sigma_{BC} & 0 \end{pmatrix},$$

$$\mathbf{D}_1 = \operatorname{diag}(\tilde{\alpha} f_A \tau_A \langle j \rangle_A, \tilde{\beta} f_B \tau_B \langle k \rangle_B, \tilde{\delta} f_C \tau_C \langle l \rangle_C),$$

$$\mathbf{D}_2 = \operatorname{diag}(\tilde{\alpha} f_A \tau_A \frac{\langle j^2 \rangle_A}{\langle j \rangle_A}, \tilde{\beta} f_B \tau_B \frac{\langle k^2 \rangle_B}{\langle k \rangle_B}, \tilde{\delta} f_C \tau_C \frac{\langle l^2 \rangle_C}{\langle l \rangle_C}).$$

Applying the Schur complement [31], the characteristic polynomial of $\mathbf{K}$ factorizes as

$$\det(\lambda \mathbf{I_6} - \mathbf{K}) = P(\lambda) Q(\lambda),$$

where

$$P(\lambda) = \det(\lambda \mathbf{I_3} - \mathbf{M}\mathbf{V}_1^{-1}),$$

$$Q(\lambda) = \det\big[\lambda I_3 - \mathbf{D}_2 \mathbf{V}_2^{-1} - (\mathbf{M}\mathbf{V}_1^{-1})(\lambda I_3 - \mathbf{M}\mathbf{V}_1^{-1})^{-1}(\mathbf{D}_1 \mathbf{V}_1^{-1})\big].$$

Expanding $P(\lambda)$ gives

$$P(\lambda) = \lambda^3 + a_1 \lambda + a_0,$$

with

$$a_1 = -\Big(\frac{\alpha_1 \beta_2 f_A f_B}{\omega_A \omega_B} \sigma_{AB} \sigma_{BA} + \frac{\alpha_2 \delta_1 f_A f_C}{\omega_A \omega_C} \sigma_{AC} \sigma_{CA} + \frac{\beta_1 \delta_2 f_B f_C}{\omega_B \omega_C} \sigma_{BC} \sigma_{CB}\Big),$$

$$a_0 = -\Big(\frac{\alpha_1 \beta_1 \delta_1 f_A f_B f_C}{\omega_A \omega_B \omega_C} \sigma_{AC} \sigma_{BA} \sigma_{CB} + \frac{\alpha_2 \beta_2 \delta_2 f_A f_B f_C}{\omega_A \omega_B \omega_C} \sigma_{AB} \sigma_{BC} \sigma_{CA}\Big).$$

Similarly, $Q(\lambda)$ is a cubic polynomial

$$Q(\lambda) = \lambda^3 + a_2 \lambda^2 + a_1' \lambda + a_0',$$

with coefficients

$$\begin{aligned}
a_2 &= -\Big(\tilde{\alpha} f_A \frac{\tau_A}{\omega_A} \frac{\langle j^2 \rangle_A}{\langle j \rangle_A} + \tilde{\beta} f_B \frac{\tau_B}{\omega_B} \frac{\langle k^2 \rangle_B}{\langle k \rangle_B} + \tilde{\delta} f_C \frac{\tau_C}{\omega_C} \frac{\langle l^2 \rangle_C}{\langle l \rangle_C}\Big), \\
a_1' &= -\alpha_1 \beta_2 f_A f_B \frac{\sigma_{AB}}{\omega_A} \frac{\sigma_{BA}}{\omega_B} \frac{\tau_A}{\omega_A} - \alpha_2 \delta_1 f_A f_C \frac{\sigma_{AC}}{\omega_A} \frac{\sigma_{CA}}{\omega_C} \frac{\tau_A}{\omega_A} \\
&\quad - \beta_1 \delta_2 f_B f_C \frac{\sigma_{BC}}{\omega_B} \frac{\sigma_{CB}}{\omega_C} \frac{\tau_B}{\omega_B} + \tilde{\alpha} \tilde{\beta} f_A f_B \frac{\tau_A}{\omega_A} \frac{\tau_B}{\omega_B} \frac{\langle j^2 \rangle_A}{\langle j \rangle_A} \frac{\langle k^2 \rangle_B}{\langle k \rangle_B} \\
&\quad + \tilde{\alpha} \tilde{\delta} f_A f_C \frac{\tau_A}{\omega_A} \frac{\tau_C}{\omega_C} \frac{\langle j^2 \rangle_A}{\langle j \rangle_A} \frac{\langle l^2 \rangle_C}{\langle l \rangle_C} + \tilde{\beta} \tilde{\delta} f_B f_C \frac{\tau_B}{\omega_B} \frac{\tau_C}{\omega_C} \frac{\langle k^2 \rangle_B}{\langle k \rangle_B} \frac{\langle l^2 \rangle_C}{\langle l \rangle_C}, \\
a_0' &= \alpha_1 \tilde{\beta} f_A f_B f_A \frac{\sigma_{AB}}{\omega_A} \frac{\sigma_{BA}}{\omega_B} \frac{\tau_A}{\omega_A} + \alpha_1 \beta_2 \tilde{\beta} f_A f_B^2 \frac{\sigma_{AB}}{\omega_A} \frac{\sigma_{BA}}{\omega_B} \frac{\tau_B}{\omega_B} \\
&\quad + \alpha_2 \tilde{\alpha} \delta_1 f_A^2 f_C \frac{\sigma_{AC}}{\omega_A} \frac{\sigma_{CA}}{\omega_C} \frac{\tau_A}{\omega_A} + \alpha_2 \tilde{\delta} \delta_1 f_A f_C^2 \frac{\sigma_{AC}}{\omega_A} \frac{\sigma_{CA}}{\omega_C} \frac{\tau_C}{\omega_C} \\
&\quad + \tilde{\alpha} \beta_1 \delta_2 f_A f_B f_C \frac{\langle j^2 \rangle_A}{\langle j \rangle_A} \frac{\sigma_{BC}}{\omega_B} \frac{\sigma_{CB}}{\omega_C} \frac{\tau_A}{\omega_A} \\
&\quad + \beta_1 \tilde{\beta} \delta_2 f_B^2 f_C \frac{\sigma_{BC}}{\omega_B} \frac{\sigma_{CB}}{\omega_C} \frac{\tau_B}{\omega_B} + \alpha_1 \beta_2 \delta_1 f_A f_B f_C \frac{\sigma_{AB}}{\omega_A} \frac{\sigma_{BC}}{\omega_B} \frac{\sigma_{CA}}{\omega_C} \\
&\quad - \alpha_1 \beta_1 \delta_1 f_A f_B f_C \frac{\sigma_{AC}}{\omega_A} \frac{\sigma_{BA}}{\omega_B} \frac{\sigma_{CB}}{\omega_C} - \alpha_2 \beta_2 \delta_2 f_A f_B f_C \frac{\sigma_{AB}}{\omega_A} \frac{\sigma_{BC}}{\omega_B} \frac{\sigma_{CA}}{\omega_C} \\
&\quad - \tilde{\alpha} \tilde{\beta} \tilde{\delta} f_A f_B f_C \frac{\langle j^2 \rangle_A}{\langle j \rangle_A} \frac{\langle k^2 \rangle_B}{\langle k \rangle_B} \frac{\langle l^2 \rangle_C}{\langle l \rangle_C} \frac{\tau_A}{\omega_A} \frac{\tau_B}{\omega_B} \frac{\tau_C}{\omega_C}.
\end{aligned}$$

where

$$f_X = \frac{\eta_X}{\eta_X + \gamma_X} \quad X \in \{A, B, C\}$$

Finally, the roots of the cubics (and thus the closed-form expression of $\mathcal{R}_0$) can be obtained by using the Cardano's formula. For a cubic equation $x^3 + ax^2 + bx + c = 0$, define the depressed cubic $y^3 + py + q = 0$ by $x = y - a/3$ with $p = b - \frac{a^2}{3}$, $q = \frac{2a^3}{27} - \frac{ab}{3} + c$, and discriminant $\Delta = (\frac{q}{2})^2 + (\frac{p}{3})^3$.

If $\Delta \geq 0$, one real root is

$$y = \sqrt[3]{-\frac{q}{2} + \sqrt{\Delta}} + \sqrt[3]{-\frac{q}{2} - \sqrt{\Delta}}. \tag{3.3}$$

If $\Delta < 0$, all three roots are real:

$$y_k = 2\sqrt{-\frac{p}{3}} \cos\Big(\frac{1}{3}\arccos\Big(\frac{3q}{2p}\sqrt{-\frac{3}{p}}\Big) - \frac{2k\pi}{3}\Big), \quad k = 0, 1, 2$$

It is easy to note that y_0 is the largest and $x = y - a/3$.

The transmission matrix F (3.2) is a nonnegative and irreducible matrix. According to the Perron–Frobenius theorem[18], its spectral radius corresponds to the largest positive eigenvalue of F. By analyzing the roots of the characteristic polynomials through Vieta's relations, we find that $P(\lambda)$ has one positive real root and two negative real roots, or one positive real root and two complex conjugate roots. Only the positive real root is relevant for our analysis; let this root be denoted by r_0.

For the polynomial $Q(\lambda)$, its three roots may consist of one positive real root and two complex roots with negative real parts, or one negative real root and two complex roots with positive real parts. In the first case, let the positive real root of $Q(\lambda)$ be r_1, and the basic reproduction number is then $\mathcal{R}_0 = \max(r_0, r_1)$. In the second case, the largest positive eigenvalue comes from $P(\lambda)$, and hence $\mathcal{R}_0 = r_0$.

Remark 3.2. To provide a more intuitive understanding, we briefly discuss the physical significance of the basic reproduction number $\mathcal{R}_0$. In the context of computer network security, $\mathcal{R}_0$ represents the expected number of secondary malware infections generated by a single compromised node introduced into a fully susceptible multi-community network during its entire infectious period. The threshold $\mathcal{R}_0 = 1$ naturally separates the extinction and persistence of the malware. From the structural composition of matrices F and V, as well as subsequent sensitivity analysis, several key influencing factors of $\mathcal{R}_0$ emerge:

Network structural heterogeneity: As reflected by the terms $\frac{\langle j^2\rangle_A}{\langle j\rangle_A}$, $\frac{\langle k^2\rangle_B}{\langle k\rangle_B}$, and $\frac{\langle l^2\rangle_C}{\langle l\rangle_C}$ in the matrix D_2, $\mathcal{R}_0$ is profoundly amplified by degree heterogeneity. High-degree nodes (hubs) act as super-spreaders, disproportionately accelerating malware propagation within their respective communities.

Intra-community vs. Inter-community Transmission: While cross-community links (σ_{XY}) provide bridges for the malware to invade secure subnetworks, intra-community infection rates (τ_X) generally exert a more dominant marginal effect on $\mathcal{R}_0$. A localized outbreak in a highly vulnerable community can elevate the overall systemic risk.

Defense expiration rate: The protection loss rates (η_X) directly modulate the pool of susceptible devices. An effective defense strategy must not only isolate infected nodes but also extend the effective duration of technical immunization to continuously suppress $\mathcal{R}_0$.

Theorem 3.3. *If $\mathcal{R}_0 < 1$, then the disease-free equilibrium (DFE) of system* (2.4) *is locally asymptotically stable.*

Proof. For the original system (2.1), it can be verified from the model formulation that the equations satisfy the biological consistency conditions (A1)–(A5) as described in [27]. According to cite[Theorem 2]van2002, when $\mathcal{R}_0 < 1$, the DFE of the infection subsystem (2.4) is locally asymptotically stable; whereas when $\mathcal{R}_0 > 1$, the DFE becomes unstable. □

Theorem 3.4. *Assume that for each community $X \in \{A, B, C\}$, the parameters satisfy*

$$\eta_X \geq \omega_X.$$

If the basic reproduction number $\mathcal{R}_0 < 1$ and the endemic equilibrium (if it exists) is unstable within the feasible region, then the disease-free equilibrium E_0 of system (2.1) *is globally asymptotically stable in the feasible region*

$$\Lambda_{3(n_A+n_B+n_C)} = \prod_{X\in\{A,B,C\}} \prod_{k=1}^{n_X} [0, 1]^3.$$

Proof. For any community $X \in \{A, B, C\}$ and degree class k, we have

$$s_k^X(t) + i_k^X(t) + p_k^X(t) = 1,$$

so we can eliminate all i_k^X by writing

$$i_k^X = 1 - s_k^X - p_k^X.$$

Substituting this into system (2.1), we obtain an autonomous system in terms of

$$\{(s_k^A, p_k^A)\}_{k=1}^{n_A}, \quad \{(s_k^B, p_k^B)\}_{k=1}^{n_B}, \quad \{(s_k^C, p_k^C)\}_{k=1}^{n_C}:$$

$$\begin{aligned}
\dot{s}_k^A &= -\alpha_1\sigma_{BA}s_k^A i^B - \alpha_2\sigma_{CA}s_k^A i^C - (1-\alpha_1-\alpha_2)k\tau_A s_k^A\Theta_i^A - \gamma_A s_k^A + \eta_A p_k^A \\
&\quad + \omega_A\big(1 - s_k^A - p_k^A\big), \\
\dot{p}_k^A &= \gamma_A s_k^A - \eta_A p_k^A, \quad k = 1, \dots, n_A, \\
\dot{s}_k^B &= -\beta_1\sigma_{CB}s_k^B i^C - \beta_2\sigma_{AB}s_k^B i^A - (1-\beta_1-\beta_2)k\tau_B s_k^B\Theta_i^B - \gamma_B s_k^B + \eta_B p_k^B \\
&\quad + \omega_B\big(1 - s_k^B - p_k^B\big), \\
\dot{p}_k^B &= \gamma_B s_k^B - \eta_B p_k^B, \quad k = 1, \dots, n_B, \\
\dot{s}_k^C &= -\delta_1\sigma_{AC}s_k^C i^A - \delta_2\sigma_{BC}s_k^C i^B - (1-\delta_1-\delta_2)k\tau_C s_k^C\Theta_i^C - \gamma_C s_k^C + \eta_C p_k^C \\
&\quad + \omega_C\big(1 - s_k^C - p_k^C\big), \\
\dot{p}_k^C &= \gamma_C s_k^C - \eta_C p_k^C, \quad k = 1, \dots, n_C,
\end{aligned} \tag{3.4}$$

where

$$\begin{aligned}
i^A &= \sum_{k=1}^{n_A} P_k^A\big(1 - s_k^A - p_k^A\big), \quad \Theta_i^A = \frac{\sum_{k=1}^{n_A} kP_k^A\big(1 - s_k^A - p_k^A\big)}{\langle k\rangle_A}, \\
i^B &= \sum_{k=1}^{n_B} P_k^B\big(1 - s_k^B - p_k^B\big), \quad \Theta_i^B = \frac{\sum_{k=1}^{n_B} kP_k^B\big(1 - s_k^B - p_k^B\big)}{\langle k\rangle_B}, \\
i^C &= \sum_{k=1}^{n_C} P_k^C\big(1 - s_k^C - p_k^C\big), \quad \Theta_i^C = \frac{\sum_{k=1}^{n_C} kP_k^C\big(1 - s_k^C - p_k^C\big)}{\langle k\rangle_C}.
\end{aligned}$$

By Theorem 3.1, $\Lambda_{3(n_A+n_B+n_C)}$ is a positively invariant set of the original system. Because of the variable relations between (2.1) and (3.4), $\Lambda_{2(n_A+n_B+n_C)}$ is a positively invariant set of system (3.4).

We denote the right-hand side of (3.4) by

$$\dot{x} = G(x), \quad x \in \Lambda_{2(n_A+n_B+n_C)},$$

where x consists of all (s_k^X, p_k^X). We compute the off-diagonal entries of the Jacobian matrix $DG(x)$. For example, in community A,

$$\dot{p}_k^A = \gamma_A s_k^A - \eta_A p_k^A$$

gives

$$\frac{\partial \dot{p}_k^A}{\partial s_k^A} = \gamma_A > 0, \quad \frac{\partial \dot{p}_k^A}{\partial x_j} = 0 \quad \text{for } x_j \neq s_k^A, p_k^A.$$

From (3.4), we have

$$\begin{aligned}
\dot{s}_k^A &= -\alpha_1\sigma_{BA}s_k^A i^B - \alpha_2\sigma_{CA}s_k^A i^C - (1-\alpha_1-\alpha_2)k\tau_A s_k^A\Theta_i^A \\
&\quad - \gamma_A s_k^A + \eta_A p_k^A + \omega_A - \omega_A s_k^A - \omega_A p_k^A.
\end{aligned}$$

Note that i^B, i^C, and Θ_i^A depend linearly on (s_k^X, p_k^X). In particular,

$$\frac{\partial \Theta_i^A}{\partial p_k^A} = -\frac{kP_k^A}{\langle k\rangle_A} < 0.$$

Hence,

$$\frac{\partial}{\partial p_k^A}\Big[-(1-\alpha_1-\alpha_2)k\tau_A s_k^A\Theta_i^A\Big] = (1-\alpha_1-\alpha_2)k^2\tau_A\frac{P_k^A}{\langle k\rangle_A}s_k^A \ \geq 0.$$

Adding the linear term

$$\frac{\partial}{\partial p_k^A}(\eta_A p_k^A - \omega_A p_k^A) = \eta_A - \omega_A,$$

we obtain

$$\frac{\partial \dot{s}_k^A}{\partial p_k^A} = (1-\alpha_1-\alpha_2)k^2\tau_A\frac{P_k^A}{\langle k\rangle_A}s_k^A + \eta_A - \omega_A.$$

Under the assumption $\eta_A \geq \omega_A$ and $s_k^A \in [0,1]$, we have

$$\frac{\partial \dot{s}_k^A}{\partial p_k^A} \geq 0.$$

For $m \neq k$, $\dot{s}_k^A$ depends on s_m^A, p_m^A only through Θ_i^A, giving

$$\frac{\partial \dot{s}_k^A}{\partial s_m^A} = (1-\alpha_1-\alpha_2)km\tau_A\frac{P_m^A}{\langle k\rangle_A}s_k^A \geq 0, \quad \frac{\partial \dot{s}_k^A}{\partial p_m^A} = (1-\alpha_1-\alpha_2)km\tau_A\frac{P_m^A}{\langle k\rangle_A}s_k^A \geq 0.$$

Since

$$i^B = \sum_r P_r^B(1-s_r^B-p_r^B),$$

we have

$$\frac{\partial i^B}{\partial s_m^B} = -P_m^B, \quad \frac{\partial i^B}{\partial p_m^B} = -P_m^B,$$

and thus

$$\frac{\partial \dot{s}_k^A}{\partial s_m^B} = \alpha_1\sigma_{BA}s_k^A P_m^B \geq 0, \quad \frac{\partial \dot{s}_k^A}{\partial p_m^B} = \alpha_1\sigma_{BA}s_k^A P_m^B \geq 0.$$

Analogous reasoning for (s_k^B, p_k^B) and (s_k^C, p_k^C) yields the same results under $\eta_B \geq \omega_B$ and $\eta_C \geq \omega_C$. Hence, under

$$\eta_X \geq \omega_X, \quad X \in \{A,B,C\},$$

and with all infection-related parameters and degree weights positive, the Jacobian matrix $DG(x)$ of system (3.4) satisfies

$$\frac{\partial G_i}{\partial x_j}(x) \geq 0, \quad i \neq j.$$

By the definition given earlier, system (3.4) is cooperative.

From the proof of Theorem 3.1, for $i_{n_X}^X > 0, X \in \{A,B,C\}$, trajectories starting on the boundary enter the interior, so we only need to consider points in $\Lambda^\circ_{2(n_A+n_B+n_C)}$, where each x satisfies the order- preserving condition.

Consider the interior

$$\Lambda^\circ_{2(n_A+n_B+n_C)} = \prod_{X\in\{A,B,C\}}\prod_{k=1}^{n_X}(0,1)^2.$$

- For each fixed community X, all degree classes (s_k^X, p_k^X) are coupled through the common mean-field term Θ_i^X, and the partial derivatives of $\dot{s}_k^X$ with respect to (s_m^X, p_m^X) are strictly positive in Λ°, so the internal directed graph is strongly connected;
- The three communities are linked through positive inter-community transmission rates σ_{XY} (e.g., i^B influences $\dot{s}_k^A$, i^A influences $\dot{s}_k^B$, etc.), connecting all variables into a single network;
- Each pair (s_k^X, p_k^X) forms a bidirectional positive feedback via $\dot{p}_k^X = \gamma_X s_k^X - \eta_X p_k^X$ and the terms $\eta_X p_k^X$, $\omega_X(1-s_k^X-p_k^X)$ in $\dot{s}_k^X$;
- Every point in $\Lambda^\circ_{2(n_A+n_B+n_C)}$ can be approximated from above and below under the partial order.

Constructing a directed graph with vertices corresponding to variables and edges $j \to i$ whenever $\partial G_i/\partial x_j(x) > 0$, the above structure ensures that for all x in $\Lambda^{\circ}_{2(n_A+n_B+n_C)}$, this graph is strongly connected. Hence, $DG(x)$ is irreducible in the interior, and the autonomous system (3.4) is strongly cooperative on $\Lambda^{\circ}_{2(n_A+n_B+n_C)}$.

By Theorem 3.3, when $\mathcal{R}_0 < 1$, the disease-free equilibrium E_0 is locally asymptotically stable in the linearized sense.

On the other hand, under the assumption that there exists no positive stable endemic equilibrium, E_0 is the unique stable equilibrium in $\Lambda_{2(n_A+n_B+n_C)}$.

In summary we have:

- System (3.4) has a compact positively invariant set $\Lambda_{2(n_A+n_B+n_C)}$;
- It is strongly cooperative on the interior $\Lambda^{\circ}_{2(n_A+n_B+n_C)}$;
- There exists a unique locally asymptotically stable equilibrium E_0.

Thus, all the hypotheses of Theorem in [24][p57,THREOM1.2] are satisfied. It follows that the set of all limit points of trajectories forms a set C that contains an open and dense subset of D. By the continuous dependence of solutions on initial conditions and the local asymptotic stability of E_0, we conclude that the disease-free equilibrium E_0 is globally asymptotically stable on $\Lambda_{2(n_A+n_B+n_C)}$. □

Remark 3.5. The assumption in Theorem 3.4 that "there exists no positive stable endemic equilibrium within the feasible region" is theoretically strong but practically necessary. In principle, if the endemic equilibrium could be explicitly characterized and its stability further analyzed, one could establish global behavior without relying on such a global assumption, using linearization or comparison principles. However, in the present model, due to the three-community structure, degree heterogeneity, and the global coupling introduced by the mean-field terms Θ_i^X, the system dimension reaches $3(n_A + n_B + n_C)$, and the endemic equilibrium equations form a highly nonlinear coupled algebraic system. Hence, a closed-form expression for the endemic equilibrium is not attainable, and its stability cannot be analyzed through standard Jacobian or Routh–Hurwitz criteria.

In the absence of explicit equilibrium expressions, the above assumption becomes a necessary prerequisite for applying the theory of strongly monotone dynamical systems. This necessity stems from the structural complexity of the model rather than from any limitation of the analytical method itself. It is worth noting that although the endemic equilibrium cannot be expressed analytically, numerical simulations show that when $\mathcal{R}_0 < 1$, regardless of the initial infection distribution, network degree distribution, or inter-community coupling configuration, all trajectories converge to the disease-free equilibrium E_0, with no persistent endemic state observed. This numerical evidence demonstrates that the global stability conclusion of the theorem is consistent with the actual dynamical behavior over a wide parameter range. Therefore, although the assumption is strong, it is both reasonable and empirically valid from the viewpoint of model behavior.

4. Numerical simulations

In this section, we present numerical investigations of the proposed model from two perspectives. First, we examine the dependence of the basic reproduction number $\mathcal{R}_0$ on various model parameters and perform sensitivity analysis to identify their relative influence. This helps determine how parameter adjustments can effectively ensure that $\mathcal{R}_0 < 1$ in practical scenarios. Subsequently, we numerically analyze the stability of the malware-free and endemic equilibria, as analytical proofs of stability are often intractable through conventional mathematical approaches, so we turn to numerical analysis.

Before presenting the specific simulation results, it is necessary to clarify the origin and selection criteria of the parameters used in this section. In practical network security applications, every parameter series in our proposed model has a concrete physical interpretation and can be estimated from empirical observation data. Specifically, the state transition rates –namely the recovery rates (ω_X), the immunization rates (γ_X), and the protection loss rates (η_X)– are defined mathematically as the inverse of their respective characteristic times: the average time required to

disinfect a compromised node, the average time to deploy a security patch to a susceptible node, and the average effective duration of a firewall rule or patch before it becomes obsolete. Conversely, the intra-community (τ_X) and inter-community (σ_{XY}) transmission probabilities are intrinsically determined by the specific virulence of the malware and the frequency of hardware or data interactions among devices. Furthermore, the proportional contribution parameters (e.g., $\alpha_1, \alpha_2, \beta_1, \beta_2$) effectively capture the inherent attack bias of the malware, quantifying how its propagation efforts are distributed between localized intra-community spread and cross-community breaches based on its specific algorithmic design. However, since the primary objective of this study is to perform a rigorous qualitative dynamical analysis rather than to fit empirical data from a specific real-world malware outbreak, the parameters utilized in our simulations are assigned representative, symbolic values based on reasonable assumptions. These values are explicitly scaled to ensure that the system encompasses both the malware-free ($\mathcal{R}_0 < 1$) and epidemic ($\mathcal{R}_0 > 1$) regimes. This approach allows us to systematically investigate the relative contributions of different structural and transmission parameters to the threshold $\mathcal{R}_0$, thereby illustrating the overarching dynamical behavior of the three-community model.

4.1. **Relationship between $\mathcal{R}_0$ and model parameters.** In this experiment, the maximum degrees of nodes in communities A, B, and C are set to 8, 10, and 12, respectively. The degree distributions in A, B, C are set uniform. For simplicity, we assume that the intra-community transmission probabilities are symmetric, i.e., $\alpha_1 = \alpha_2$, $\beta_1 = \beta_2$, and $\delta_1 = \delta_2 = a$. The parameter δ is held fixed, as our numerical experiments focus on examining the dependence of $\mathcal{R}_0$ on α and β, and visualizing more than three varying parameters within a single figure would be impractical. The cross-community transmission probabilities between communities are set to $\sigma_{BA} = \sigma_{CA} = 0.4$, $\sigma_{AB} = \sigma_{CB} = 0.3$, and $\sigma_{AC} = \sigma_{BC} = 0.2$. Moreover, the recovery and protection rates are assumed to be identical across all communities, with $\gamma_A = \gamma_B = \gamma_C = 0.2$, $\eta_A = \eta_B = \eta_C = 0.1$, and $\omega_A = \omega_B = \omega_C = 0.4$.

We find that the relationship between the basic reproduction number $\mathcal{R}_0$ and the parameters α and β is non-monotonic (i.e., $\mathcal{R}_0$ may either increase or decrease as α or β varies), as illustrated in Figure 3. This implies that restricting the interconnections among susceptible individuals within a community has a complex influence on the magnitude of $\mathcal{R}_0$. Therefore, simply limiting intra-community connections among susceptible nodes may not be an effective strategy for malware containment, and other factors should be taken into account when designing protective measures.

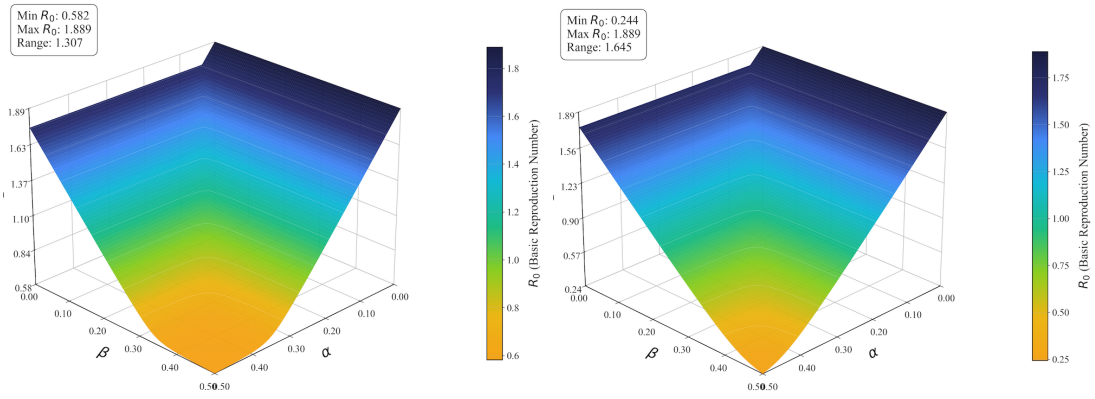

FIGURE 3. Colormaps of $\mathcal{R}_0$ with respect to α and β under a fixed δ. $\delta = 0.3$ (left), $\delta = 0.5$ (right)

To further illustrate the critical relationship between α and β when $\mathcal{R}_0 = 1$, we plot in Figure 4 the contour lines corresponding to $\mathcal{R}_0 = 1$. The upper-right region enclosed by the contour represents the parameter space in which malware transmission can be effectively controlled.

To investigate the sensitivity of the basic reproduction number $\mathcal{R}_0$ with respect to various parameters, we adopt a generalized model in which the effects of α, β, and δ associated with

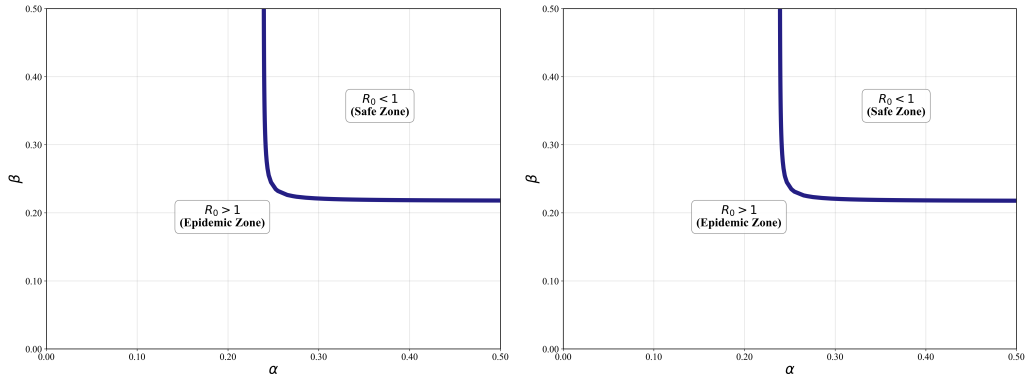

FIGURE 4. Contours of α and β when $\mathcal{R}_0 = 1$ under a fixed δ. $\delta = 0.3$ (left), $\delta = 0.5$ (right).

intra-community transmission are disregarded. Specifically, we aggregate the intra-community contribution into a single parameter $\tilde{\alpha}$ by replacing $1 - \alpha_1 - \alpha_2$ with a new parameter $\tilde{\alpha}$. The same treatment is applied to β and δ. Based on these adjustments, we obtain the following generalized model:

$$\begin{aligned}
\dot{s}_k^A &= -\alpha_1\sigma_{BA}s_k^A i_B - \alpha_2\sigma_{CA}s_k^A i_C - \tilde{\alpha}k\tau_A s_k^A\Theta_i^A - \gamma_A s_k^A + \eta_A p_k^A + \omega_A i_k^A,\\
\dot{i}_k^A &= \alpha_1\sigma_{BA}s_k^A i_B + \alpha_2\sigma_{CA}s_k^A i_C + \tilde{\alpha}k\tau_A s_k^A\Theta_i^A - \omega_A i_k^A,\\
\dot{p}_k^A &= \gamma_A s_k^A - \eta_A p_k^A,\\
\dot{s}_k^B &= -\beta_1\sigma_{CB}s_k^B i_C - \beta_2\sigma_{AB}s_k^B i_A - \tilde{\beta}k\tau_B s_k^B\Theta_i^B - \gamma_B s_k^B + \eta_B p_k^B + \omega_B i_k^B,\\
\dot{i}_k^B &= \beta_1\sigma_{CB}s_k^B i_C + \beta_2\sigma_{AB}s_k^B i_A + \tilde{\beta}k\tau_B s_k^B\Theta_i^B - \omega_B i_k^B,\\
\dot{p}_k^B &= \gamma_B s_k^B - \eta_B p_k^B,\\
\dot{s}_k^C &= -\delta_1\sigma_{AC}s_k^C i_A - \delta_2\sigma_{BC}s_k^C i_B - \tilde{\delta}k\tau_C s_k^C\Theta_i^C - \gamma_C s_k^C + \eta_C p_k^C + \omega_C i_k^C,\\
\dot{i}_k^C &= \delta_1\sigma_{AC}s_k^C i_A + \delta_2\sigma_{BC}s_k^C i_B + \tilde{\delta}k\tau_C s_k^C\Theta_i^C - \omega_C i_k^C,\\
\dot{p}_k^C &= \gamma_C s_k^C - \eta_C p_k^C.
\end{aligned} \tag{4.1}$$

$$F = \begin{pmatrix}
0 & \alpha_1 f_A\sigma_{BA} & \alpha_2 f_A\sigma_{CA} & \tilde{\alpha}f_A\tau_A\langle j\rangle_A & 0 & 0\\
\beta_2 f_B\sigma_{AB} & 0 & \beta_1 f_B\sigma_{CB} & 0 & \tilde{\beta}f_B\tau_B\langle k\rangle_B & 0\\
\delta_1 f_C\sigma_{AC} & \delta_2 f_C\sigma_{BC} & 0 & 0 & 0 & \tilde{\delta}f_C\tau_C\langle l\rangle_C\\
0 & \alpha_1 f_A\sigma_{BA} & \alpha_2 f_A\sigma_{CA} & \tilde{\alpha}f_A\tau_A\frac{\langle j^2\rangle_A}{\langle j\rangle_A} & 0 & 0\\
\beta_2 f_B\sigma_{AB} & 0 & \beta_1 f_B\sigma_{CB} & 0 & \tilde{\beta}f_B\tau_B\frac{\langle k^2\rangle_B}{\langle k\rangle_B} & 0\\
\delta_1 f_C\sigma_{AC} & \delta_2 f_C\sigma_{BC} & 0 & 0 & 0 & \tilde{\delta}f_C\tau_C\frac{\langle l^2\rangle_C}{\langle l\rangle_C}
\end{pmatrix} \tag{4.2}$$

$$f_X = \frac{\eta_X}{\eta_X + \gamma_X} \quad X \in \{A, B, C\}$$

For the baseline setting, we set $\alpha = \beta = \delta = 0.3$ and $\tilde{\alpha} = \tilde{\beta} = \tilde{\delta} = 0.4$, and then numerically compute the partial derivatives of $\mathcal{R}_0$ with respect to multiple parameters using the explicit expression of $\mathcal{R}_0$ derived from the polynomials and (3.3). The results are shown in Fig 5.

From Figure 5, it can be observed that $\mathcal{R}_0$ exhibits substantially higher sensitivity to $\tilde{\alpha}$, $\tilde{\beta}$, and $\tilde{\delta}$ than to α, β, and δ. This suggests that intra-group transmission plays a more critical role in the transmission dynamics and thus warrants greater attention. Furthermore, among the inter-community parameters, α shows a stronger influence on $\mathcal{R}_0$ than β and δ.

Building upon the above sensitivity analysis of $\mathcal{R}_0$ with respect to α and β, we further explore its dependence on other essential parameters, including η, ω, τ, and σ, which characterize the recovery and transmission capabilities of nodes. Unless otherwise stated in the figures, all parameter settings

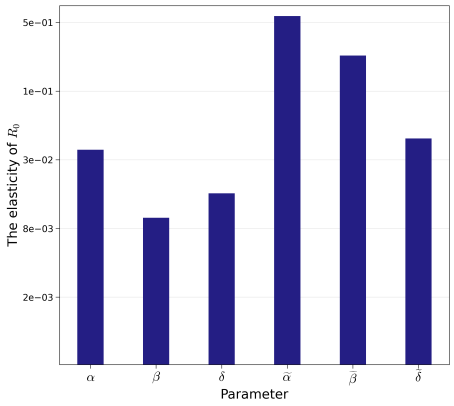

FIGURE 5. The figure shows the elasticity of $\mathcal{R}_0$ with respect to α, β, δ and $\tilde{\alpha}$, $\tilde{\beta}$, $\tilde{\delta}$ under uniform distribution.

remain consistent with those in the previous experiments. The network topology is modeled using either a power-law or a Poisson degree distribution to capture the heterogeneity of connectivity patterns in real-world networks.

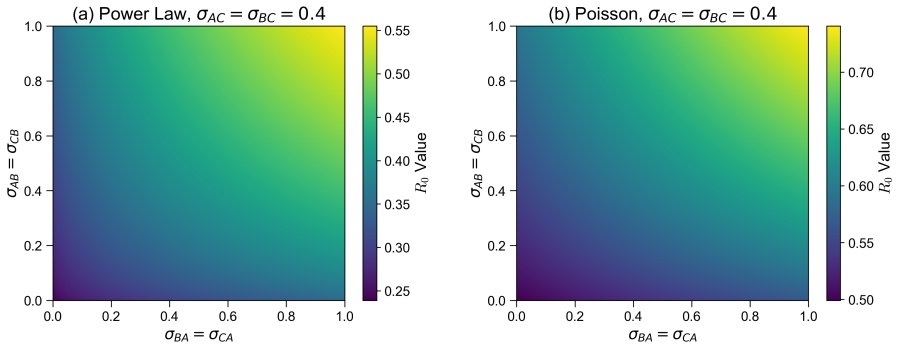

FIGURE 6. The figure shows how much $\mathcal{R}_0$ is under fixed $\sigma_{AC} = \sigma_{BC}$ and different $\sigma_{BA} = \sigma_{CA}$ and $\sigma_{CB} = \sigma_{AB}$. The left figure follows power law, while the right follows poisson distribution.

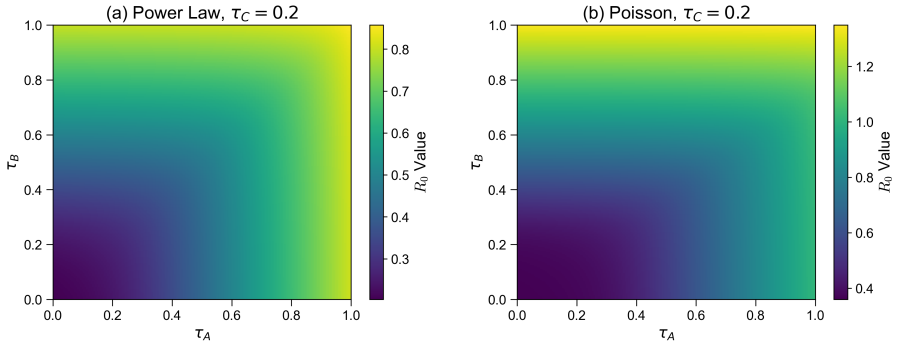

FIGURE 7. The figure shows how much $\mathcal{R}_0$ is under fixed τ_C and different τ_A and τ_B. The left figure follows power law, while the right follows poisson distribution.

A detailed comparison of the figures reveals several notable features. Except for Figure 7, the overall structure of the colormaps remains nearly unchanged, although the magnitude of $\mathcal{R}_0$ varies

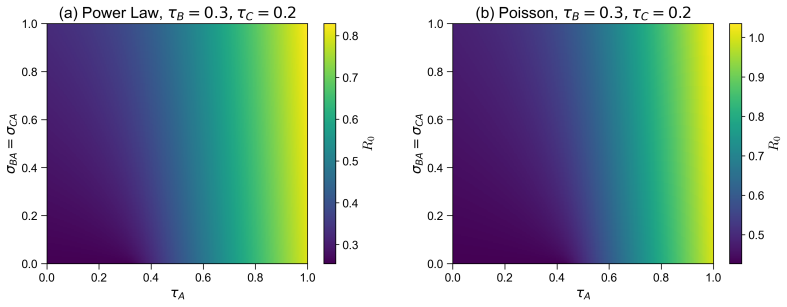

FIGURE 8. The figure shows how much $\mathcal{R}_0$ is under fixed τ_C and τ_B and different τ_A and $\sigma_{BA} = \sigma_{CA}$. The left figure follows power law, while the right follows poisson distribution.

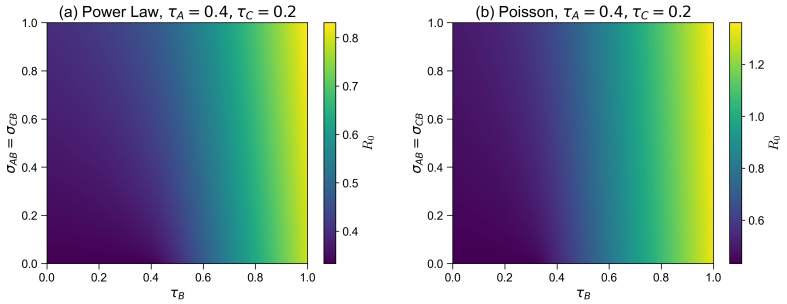

FIGURE 9. The figure shows how much $\mathcal{R}_0$ is under fixed τ_A and τ_C and different τ_B and $\sigma_{AB} = \sigma_{CB}$. The left figure follows power law, while the right follows poisson distribution.

significantly. Under the Poisson degree distribution, the values of $\mathcal{R}_0$ are consistently higher and more likely to exceed the critical threshold $\mathcal{R}_0 = 1$. In Figure 7, $\mathcal{R}_0$ attains its maximum when both τ_A and τ_B approach 1.

Furthermore, comparing Figure 8 with Figure 9 shows that, for power-law networks, $\mathcal{R}_0$ exhibits similar spatial distributions under parameter pairs $(\tau_A, \sigma_{BA} = \sigma_{CA})$ and $(\tau_B, \sigma_{AB} = \sigma_{CB})$. In contrast, within Poisson networks, variations in the parameters of community B lead to a more pronounced increase in $\mathcal{R}_0$.

From Figure 10, it is evident that community A, being more susceptible to malware, also exerts the greatest influence on the sensitivity of $\mathcal{R}_0$. Under the power-law degree distribution, the ordering $\tau_A > \tau_B > \tau_C$ corresponds to the gradient relation

$$\frac{\partial \mathcal{R}_0}{\partial \tau_A} > \frac{\partial \mathcal{R}_0}{\partial \tau_B} > \frac{\partial \mathcal{R}_0}{\partial \tau_C},$$

indicating that higher transmission capability within a more vulnerable community yields a greater marginal effect on $\mathcal{R}_0$. A similar pattern is observed for the parameters $\boldsymbol{\sigma}$.

4.2. **Stability of the malware-free equilibrium.** We first verify that when $\mathcal{R}_0 < 1$, the malware-free equilibrium is globally asymptotically stable, in agreement with the results reported in Theorem 3.3. Furthermore, for the specific parameter values and initial conditions tested below, our numerical simulations show that the system converges to this equilibrium.

It is worth noting that, unless stated otherwise, all parameters are fixed at the values specified above. Initial conditions are chosen as $(s_X^k, i_X^k, p_X^k) = (1 - i_0, i_0, 0)$ for $X = \{A, B, C\}$. Only the community maximal degree k_X and initial infected computers ratio i_X^k for $X = \{A, B, C\}$ are varied for convenience, as larger community maximal degrees generally lead to higher values of $\mathcal{R}_0$.

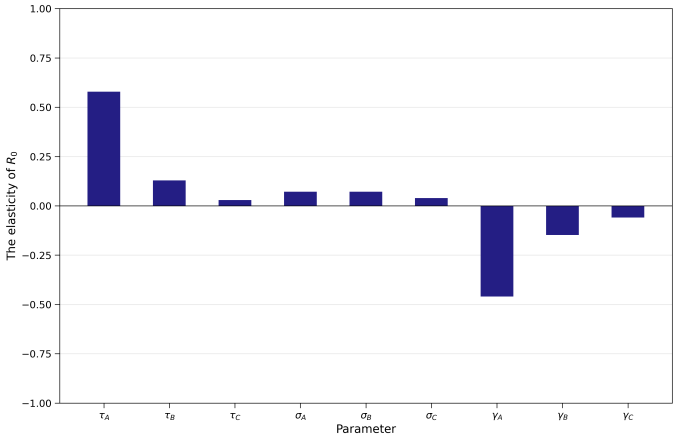

FIGURE 10. The figure shows the sensitivity of $\mathcal{R}_0$ to spread and recovery parameters under power law.

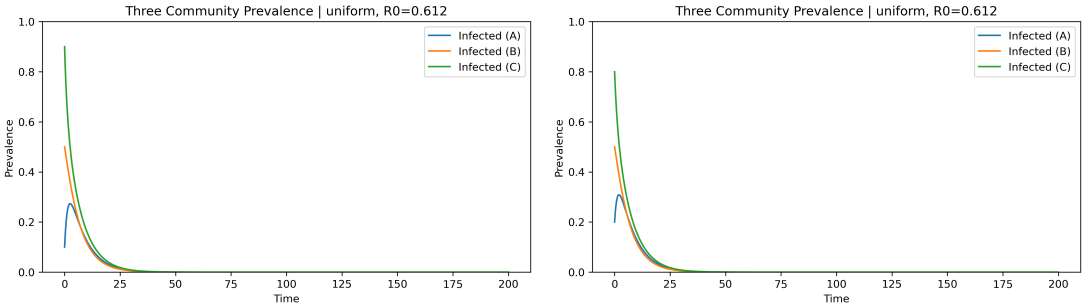

FIGURE 11. Dynamics of infected computers in the three communities under the uniform distribution. The basic reproduction number of the system is $\mathcal{R}_0 = 0.612$. The initial values are $(i_A^k, i_B^k, i_C^k) = (0.1, 0.5, 0.9)$ (left) and $(0.2, 0.5, 0.8)$ (right).

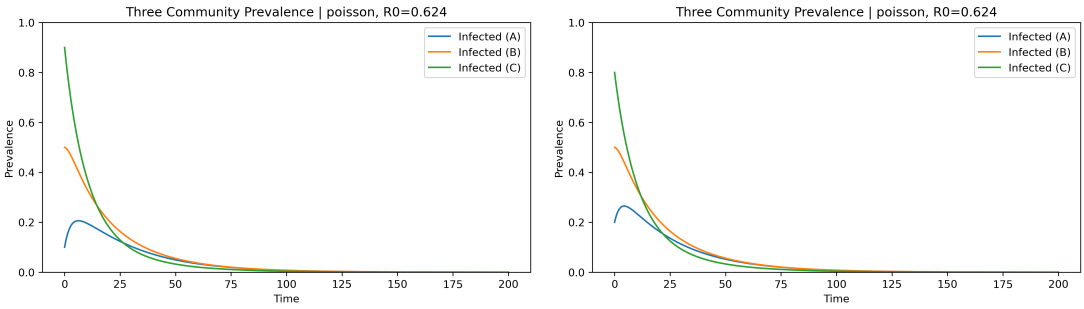

FIGURE 12. Dynamics of infected computers in the three communities under the Poisson distribution. The system has $\mathcal{R}_0 = 0.624$. The initial values are $(i_A^k, i_B^k, i_C^k) = (0.1, 0.5, 0.9)$ (left) and $(0.2, 0.5, 0.8)$ (right), with $k_A = 2$, $k_B = 2$, $k_C = 3$.

Figures 11–13 illustrate that, irrespective of whether the initial conditions are $(i_A^k, i_B^k, i_C^k) = (0.1, 0, 5, 0, 9)$ or $(0.2, 0.5, 0.8)$, and regardless of whether the degree distribution is uniform, Poisson, or power-law, the system asymptotically converges to the malware-free equilibrium. These results confirm the asymptotic stability of the equilibrium and provide additional support for our

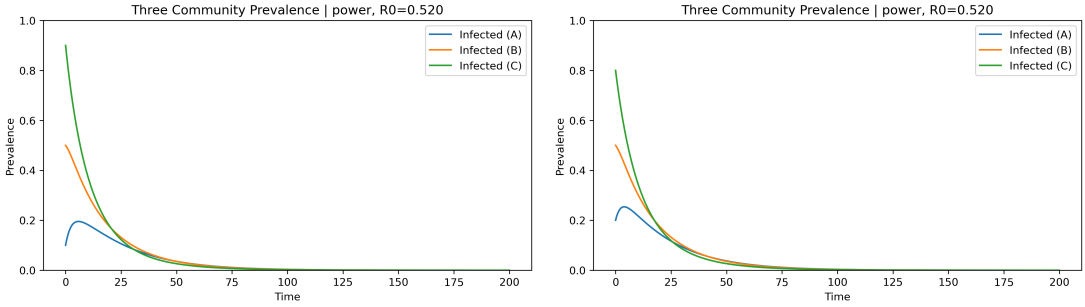

FIGURE 13. Dynamics of infected computers in the three communities under the power-law distribution. The system has $\mathcal{R}_0 = 0.520$. The initial values are $(i_A^k, i_B^k, i_C^k) = (0.1, 0.5, 0.9)$ (left) and $(0.2, 0.5, 0.8)$ (right), with $k_A = 2$, $k_B = 2$, $k_C = 3$.

conjecture of its global stability. Notably, even when the initial proportion of infected nodes is high, the system is capable of eliminating the malware autonomously.

As shown in Figures. 11–13, regardless of whether the initial conditions are set as $(i_A^k, i_B^k, i_C^k) = (0.1, 0.5, 0.9)$ or $(0.2, 0.5, 0.8)$, and regardless of whether the network degree distribution follows a uniform, Poisson, or power-law form, the system eventually converges to the malware-free equilibrium. By examining the temporal decay of the infection density, we observe that the convergence time to the steady state varies substantially across different degree distributions. Under the homogeneous degree distribution, the infection densities in the three communities decay at the fastest rate and converge to zero within a short time interval. Moreover, the corresponding trajectories of the communities nearly coincide throughout the evolution, indicating a high level of synchronization. This implies that, in networks with homogeneous connectivity, the infection dynamics across communities evolve on comparable time scales and exhibit similar asymptotic behavior.

In contrast, for Poisson and power-law degree distributions, the decay of the infection density is significantly slower. The system exhibits pronounced long-tail transient dynamics before reaching the steady state, and the trajectories associated with different communities show noticeable deviations. This reflects a desynchronization in the infection dynamics, with heterogeneous degree distributions inducing multiple characteristic time scales and non-uniform convergence across communities.

4.3. **Stability of the endemic equilibrium.** In this section, we first describe the numerical procedure for computing the malware-infected equilibrium. We then present evidence supporting our conjecture that this equilibrium is locally asymptotically stable, though our numerical experiments suggest potential global convergence.

To begin, we replace the variables s and Θ_s in the formulas with i and Θ_i to ensure self-consistency in the equations. By substituting the equilibrium expressions for the protected nodes in the model and applying the fundamental conservation of proportions: At equilibrium for the protected nodes, we have $\dot{p}_k^X = \gamma_X s_k^X - \eta_X p_k^X = 0$ implies $p_k^X = \frac{\gamma_X}{\eta_X} s_k^X$, and by the normalization condition, $s_k^X + i_k^X + p_k^X = 1$.

We then introduce the new variables: $\rho_X = \frac{\eta_X}{\eta_X + \gamma_X}$ and $\kappa_X = \frac{\langle k^2 \rangle_X}{\langle k \rangle_X}$, which allow us to rewrite the susceptible fraction and the mean-field term as

$$s^X = \rho_X(1 - i^X), \quad \Theta_s^X = \rho_X(1 - \Theta_i^X).$$

We then obtain the self-consistent differential equations in the malware-infected equilibrium:

$$\begin{aligned}
\dot{i}_A &= \alpha_1\sigma_{BA}\,\rho_A(1-i_A)i_B + \alpha_2\sigma_{CA}\,\rho_A(1-i_A)i_C \\
&\quad + (1-\alpha_1-\alpha_2)\,\langle j\rangle_A\,\tau_A\,\rho_A\,(1-\Theta_i^A)\Theta_i^A - \omega_A i_A, \\
\dot{i}_B &= \beta_1\sigma_{CB}\,\rho_B(1-i_B)i_C + \beta_2\sigma_{AB}\,\rho_B(1-i_B)i_A \\
&\quad + (1-\beta_1-\beta_2)\,\langle k\rangle_B\,\tau_B\,\rho_B\,(1-\Theta_i^B)\Theta_i^B - \omega_B i_B, \\
\dot{i}_C &= \delta_1\sigma_{AC}\,\rho_C(1-i_C)i_A + \delta_2\sigma_{BC}\,\rho_C(1-i_C)i_B \\
&\quad + (1-\delta_1-\delta_2)\,\langle \ell\rangle_C\,\tau_C\,\rho_C\,(1-\Theta_i^C)\Theta_i^C - \omega_C i_C, \\
\dot{\Theta}_i^A &= \alpha_1\sigma_{BA}\,\rho_A(1-\Theta_i^A)i_B + \alpha_2\sigma_{CA}\,\rho_A(1-\Theta_i^A)i_C \\
&\quad + (1-\alpha_1-\alpha_2)\,\tau_A\,\rho_A\,\kappa_A(1-i_A)\Theta_i^A - \omega_A\Theta_i^A, \\
\dot{\Theta}_i^B &= \beta_1\sigma_{CB}\,\rho_B(1-\Theta_i^B)i_C + \beta_2\sigma_{AB}\,\rho_B(1-\Theta_i^B)i_A \\
&\quad + (1-\beta_1-\beta_2)\,\tau_B\,\rho_B\,\kappa_B(1-i_B)\Theta_i^B - \omega_B\Theta_i^B, \\
\dot{\Theta}_i^C &= \delta_1\sigma_{AC}\,\rho_C(1-\Theta_i^C)i_A + \delta_2\sigma_{BC}\,\rho_C(1-\Theta_i^C)i_B \\
&\quad + (1-\delta_1-\delta_2)\,\tau_C\,\rho_C\,\kappa_C(1-i_C)\Theta_i^C - \omega_C\Theta_i^C.
\end{aligned} \tag{4.3}$$

By setting the left-hand side of equation 4.3 to zero, the equilibrium $(i_A, i_B, i_C, \Theta_i^A, \Theta_i^B, \Theta_i^C)$ can be computed by reducing the high-dimensional model to the six-dimensional system in equation 4.3. This system is effectively quadratic, allowing for rapid solution using Newton's method[12].

Although a closed-form expression for the equilibrium is generally not available, a numerical solution can be obtained. This enables transformation of the system to its equilibrium state and computation of the basic reproduction number at equilibrium. Such a procedure allows verification of the asymptotic stability of the system under specific parameter configurations.

To further support our conjecture regarding the global stability of the malware-infected equilibrium, we examine scenarios in which $\mathcal{R}_0 > 1$ under various degree distributions. The results are shown in Figure 14, 15 and 16

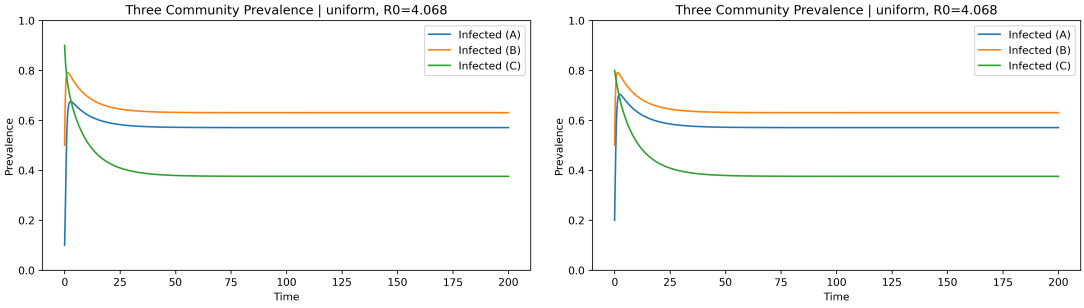

FIGURE 14. Dynamics of infected computers in the three communities under the uniform distribution. The system has $\mathcal{R}_0 = 4.068$. The initial values are $(i_A^k, i_B^k, i_C^k) = (0.1, 0.5, 0.9)$ (left) and $(0.2, 0.5, 0.8)$(right), with $k_A = 20$, $k_B = 30$, $k_C = 40$.

Different degree distributions alter the structural heterogeneity of the network and thereby exert a significant influence on the evolution of spreading dynamics. Under a homogeneous degree distribution, the network structure is relatively regular, and the roles of individual nodes in the spreading process are approximately equivalent, leading to a smooth temporal evolution of the infection proportion.

For the Poisson degree distribution, node degrees in the network exhibit random fluctuations. Numerical results indicate that the system reaches the steady state more rapidly, and the steady-state infection levels across different communities are close to each other, allowing the spreading process to diffuse more uniformly throughout the network.

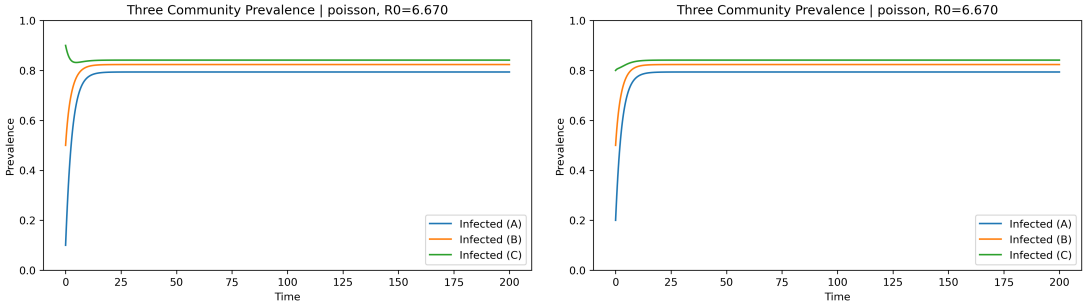

FIGURE 15. Dynamics of infected computers in the three communities under the Poisson distribution. The system has $\mathcal{R}_0 = 6.670$. The initial values are $(i_A^k, i_B^k, i_C^k) = (0.1, 0.5, 0.9)$ (left) and $(0.2, 0.5, 0.8)$(right), with $k_A = 10$, $k_B = 12$, $k_C = 16$.

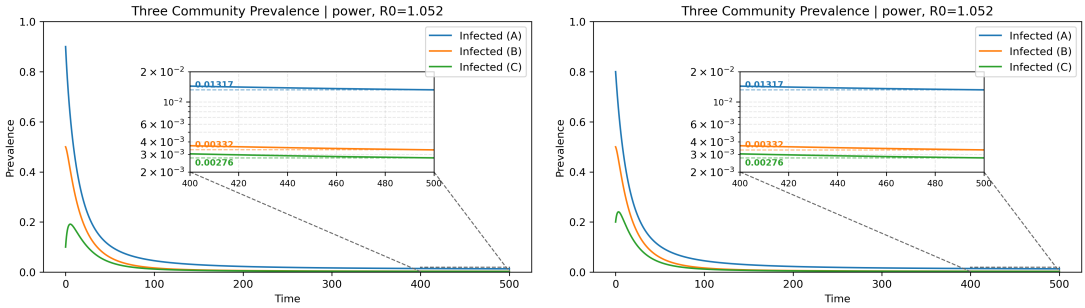

FIGURE 16. Dynamics of infected computers in the three communities under the power-law distribution. The system has $\mathcal{R}_0 = 1.052$. The initial values are $(i_A^k, i_B^k, i_C^k) = (0.1, 0.5, 0.9)$ (left) and $(0.2, 0.5, 0.8)$(right), with $k_A = 20$, $k_B = 10$, $k_C = 20$.

Under the power-law degree distribution, although a small number of high-degree nodes exhibit relatively high infection proportions, the majority of low-degree nodes maintain low infection levels. As a consequence, the overall average infection level remains low. This phenomenon reflects a non-uniform steady-state structure in which the spreading dynamics are primarily sustained by high-degree (hub) nodes. This observation is consistent with existing studies showing that spreading processes in heterogeneous networks are dominated by hub nodes.

REFERENCES

[1] M. Akbanov, V. G. Vassilakis, M. D. Logothetis; *Wannacry ransomware: Analysis of infection, persistence, recovery prevention and propagation mechanisms*, Journal of Telecommunications and Information Technology, **75** (2019), no. 1, 113–124.

[2] H. AL-Mohannadi, Q. Mirza, A. Namanya, I. Awan, A. Cullen, J. Disso; *Cyberattack modeling analysis techniques: An overview*, 2016 4th International Conference on Future Internet of Things and Cloud Workshops, 2016, pp. 324–329.

[3] N. T. J. Bailey; *The mathematical theory of infectious diseases and its applications*, Oxford University Press, New York, 1975.

[4] S. Boccaletti, V. Latora, Y. Moreno, M. Chavez, D.-U. Hwang; *Complex networks: structure and dynamics*, Physics Reports **424** (2006), 175–308.

[5] A. Chernikova, N. Gozzi, N. Perra, S. Boboila, T. Eliassi-Rad, A. Oprea; *Modeling self-propagating malware with epidemiological models*, Applied Network Science, **8** (2023), no. 1, 52.

[6] Thomas Ciza, N. Balakrishnan; *Performance enhancement of intrusion detection systems using advances in sensor fusion*, Proceedings of the 11th International Conference on Information Fusion, 6 2008, pp. 1–7.

[7] L. Feng, X. Liao, Q. Han, H. Li; *Dynamical analysis and control strategies on malware propagation model*, Applied Mathematical Modelling **37** (2013), no. 18-19, 8225–8236.

[8] M. Garetto, W. B. Gong, D. Towsley; *Modeling malware spreading dynamics*, Proceedings of the 22nd Annual Joint Conference of the IEEE Computer and Communications (INFOCOM 2003), vol. 3, 2003, pp. 1869–1879.
[9] J. D. Hernández Guillén, A. Martín del Rey, R. Casado-Vara, *Security countermeasures of a sciras model for advanced malware propagation*, IEEE Access **7** (2019), 135472–135477.
[10] H. W. Hethcote; *The mathematics of infectious diseases*, SIAM Review, **42** (2000), 599.
[11] S. Hosseini, M. A. Azgomi; *A model for malware propagation in scale-free networks based on rumor spreading process*, Computer Networks, **106** (2016), 57–67.
[12] C. T. Kelley; *Iterative methods for linear and nonlinear equations*, Frontiers in Applied Mathematics, vol. 16, SIAM, 1995.
[13] J. O. Kephart, S. R. White; *Directed-graph epidemiological models of computer viruses*, Proceedings of the IEEE Computer Society Symposium on Security and Privacy (Oakland, CA, USA), IEEE Computer Society, 1991, pp. 343–359.
[14] M. H. R. Khouzani, Saswati Sarkar, Eitan Altman; *Maximum damage malware attack in mobile wireless networks*, IEEE/ACM Transactions on Networking **20** (2012), no. 5, 1347–1360.
[15] Labs; *Notpetya technical analysis*, 2017, Accessed: 2025-09-02 [Online].
[16] C. H. Li, C. C. Tsai, S. Y. Yang; *Analysis of epidemic spreading of an sirs model in complex heterogeneous networks*, Communications in Nonlinear Science and Numerical Simulation, **19** (2014), no. 4, 1042–1054.
[17] Wanping Liu, Chao Liu, Zheng Yang, Xiaoyang Liu, Yihao Zhang, Zuxue Wei; *Modeling the propagation of mobile malware on complex networks*, Commun Nonlinear Sci Numer Simulat, **37** (2016), 249–264.
[18] Carl D. Meyer; *Matrix analysis and applied linear algebra*, Society for Industrial and Applied Mathematics, Philadelphia, 2000, See Chapter 8 for the Perron-Frobenius theorem.
[19] B. K. Mishra, N. Jha; *Seiqrs model for the transmission of malicious objects in computer network*, Applied Mathematical Modelling **34** (2010), no. 11, 3451–3458.
[20] Y. Moreno, R. Pastor-Satorras, A. Vespignani; *Epidemic outbreaks in complex heterogeneous networks*, The European Physical Journal B, **26** (2002), no. 4, 521–529.
[21] M. Nekovee; *Worm epidemics in wireless ad hoc networks*, New Journal of Physics, **9** (2007), 189.
[22] R. Pastor-Satorras A. Vespignani; *Epidemic spreading in scale-free networks*, Physical Review Letters, **86** (2001), no. 14, 3200–3203.
[23] A. Singh, Y. N. Singh; *Nonlinear spread of rumor and inoculation strategies in the nodes with degree dependent tie strength in complex networks*, Acta Physica Polonica B, **44** (2013), no. 1, 5–28.
[24] Hal L. Smith; *Monotone dynamical systems: An introduction to the theory of competitive and cooperative systems*, Mathematical Surveys and Monographs, vol. 41, American Mathematical Society, Providence, RI, 1995.
[25] S. Sundar, S. N. Tewari, N. Swaroop; *Understanding virus propagation in computer networks and strengthening security with antivirus programs for a safer society: A mathematical study*, Proceedings of ICMLCS 2024, 2024, pp. 451–467.
[26] Shyam Sundar, Sumiti Narayan Tewari, Niranjan Swaroop; *Understanding virus propagation in computer networks and strengthening security with antivirus programs for a safer society: A mathematical study*, Mathematics and Logics in Computer Science: Proceedings of ICMLCS 2024 (Atul Chaturvedi, Bimal Kumar Roy, and Boaz Tsaban, eds.), Algorithms for Intelligent Systems, Springer Nature Singapore Pte Ltd., Singapore, 2025, pp. 451–467.
[27] P. van den Driessche, J. Watmough; *Reproduction numbers and sub-threshold endemic equilibria for compartmental models of disease transmission*, Mathematical Biosciences, **180** (2002), no. 1-2, 29–48.
[28] J. Wang, L. Zhao, R. Huang; *2si2r rumor spreading model in homogeneous networks*, Physica A **413** (2014), 153–161.
[29] H. Xue, Y. Wang, Q. Tang; *Dynamic analysis of malicious behavior propagation based on feature selection in software network*, Frontiers in Physics, **12** (2024), 1493209.
[30] James A. Yorke; *Invariance for ordinary differential equations*, Mathematical Systems Theory, **1** (1967), no. 4, 353–372.
[31] Fuzhen Zhang; *The schur complement and its applications*, Springer, New York, 2005.
[32] C. C. Zou, W. Gong, D. Towsley; *Code red worm propagation modeling and analysis*, Proceedings of the 9th ACM Conference on Computer and Communications Security (CCS), ACM, 2002, pp. 138–147.

Ziheng Cheng
School of Mathematical Sciences, Shanghai Jiao Tong University, Shanghai 200240, China
Email address: harryczh@sjtu.edu.cn

Hanqing Hu
School of Mathematical Sciences, Shanghai Jiao Tong University, Shanghai 200240, China
Email address: hhqhaha666@sjtu.edu.cn

Teng Ma
School of Mathematical Sciences, Shanghai Jiao Tong University, Shanghai 200240, China
Email address: dlutecnu@sjtu.edu.cn

Huangjie Zheng
School of Mathematical Sciences, Shanghai Jiao Tong University, Shanghai 200240, China
Email address: huangjie7796@sjtu.edu.cn